Theory for the evolution of ferroelectric, antiferroelectric, and ferrielectric smectic phases in the electric field

A. V. Emelyanenko*
Department of Physics, Moscow State University, Moscow 119991, Russia
(Received 17 March 2010; revised manuscript received 3 September 2010; published 28 September 2010)

An evolution of Sm-C_A^*, biaxial intermediate phases, and Sm-C^* in the electric field is investigated in a framework of molecular-statistical approach [A. V. Emelyanenko *et al.*., Phys. Rev. E **74**, 011705 (2006); A. V. Emelyanenko, Eur. Phys. J. E **28**, 441 (2009)]. The "electric field–temperature" phase diagrams including the possibility of existence of various tilted smectic phases are plotted and compared with the experimental ones. Permanent transverse molecular dipole moments (without electric field participating only in the spontaneous polarization) were also found to generate the induced polarization in the presence of electric field and to produce very strong dielectriclike effect. This effect is positive in Sm-C^* (tilt planes have a tendency of orienting along or against the electric field) and is negative in Sm-C_A^* and in biaxial intermediate phases (tilt planes have a tendency of orienting perpendicular to the electric field). In the ferrielectric intermediate phases both spontaneous and induced polarizations favor similar tendencies and provide the helix unwinding at very low electric field. At the same time, the tendencies provided by spontaneous and induced polarizations are opposite in Sm-C^*, and therefore the unwinding threshold is larger. It was shown that interplay between spontaneous and induced polarizations can lead to the formation of complex bidomain smectic structures. A single parameter regulating an evolution of structure of Sm-C^*, Sm-C_A^*, and biaxial intermediate phases in the electric field was found. We suppose that bidomain helical structure is the same as additional ferrielectric phase FiLC existing in some materials just below Sm-C^*. The numerical calculations are done with help of AFLC phase diagram plotter software developed by the author and available at his webpage.

DOI: 10.1103/PhysRevE.82.031710 PACS number(s): 61.30.Cz, 64.70.M−

I. INTRODUCTION

Evolution of various tilted smectic phases in the electric field is an interesting problem not only from the fundamental point of view, but also for possible applications of new smectic phases in display industry, production of various detectors, light modulators, switchers, etc. The possibility of existence of *several* tilted smectic phases in the same material at various temperatures was discovered for the first time in [1,2]. The anticlinic antiferroelectric Sm-C_A^* phase was confirmed in a liquid crystal, MHPOBC, by observing the switching current due to the in-layer polarization reversal together with the disappearance of the so-called full-pitch reflection band due to the helical structure, which clearly emerges in synclinic ferroelectric Sm-C^*. In addition, MHPOBC material appeared to possess two subphases, designated at that time as Sm-C_α^* and Sm-C_γ^*. Optically uniaxial Sm-C_α^* emerges just below Sm-A^*, while optically biaxial Sm-C_γ^* appears between Sm-C_A^* and Sm-C^*. The molecular orientational structure of Sm-C_γ^* was clarified to be *ferrielectric* by studying the electric field dependence of conoscopic figures [3]. Analysis of the macroscopic helical pitch and the switching characteristics in Sm-C_γ^* resulted in the detailed structure consisting of a unit cell with three-layer periodicity that contains the ferroelectric and antiferroelectric orderings in a ratio of 1:2 [4,5]. The macroscopic helical pitch was estimated from optical rotatory power and liquid-crystal-induced circular dichroism [4,6]. This was a surprising and fundamental condensed-matter finding and prompted intensive research into the structure and properties.

Later an intermediate antiferroelectric phase other than Sm-C_A^* was found between Sm-C_γ^* and Sm-C_α^* in MHPBC, the molecular structure of which is the same as that of MHPOBC except in the removal of only one oxygen atom from the achiral chain. Studying the electric field dependence of conoscopic figures leads to a conclusion that the macroscopic helical pitches in the new antiferroelectric phase (simply designated as AF) as well as Sm-C_γ^* are extremely long [7]. Further systematic investigations were made by Isozaki *et al.* and clarified that the aforementioned subphases, Sm-C_γ^*, AF, and Sm-C_α^*, together with two additional ones below and above Sm-C_γ^* (designated as FI_L and FI_H, respectively), were found in several single compounds and mixtures [8,9]. In this way, it was well noticed that the frustration between ferroelectricity and antiferroelectricity produces a series of biaxial intermediate phases (see Fig. 1), which can be specified by parameter q_T denoting the fraction of almost synclinic orderings in particular phase. Thus, the fraction of almost anticlinic orderings in the same phases is $1-q_T$. Since all of these biaxial subphases are based on the existence of Sm-C_A^*, Isozaki *et al.* appropriately proposed to designate them as Sm-$C_A^*(q_T)$'s. Thus, two prototype subphases, Sm-C_γ^* and AF, are Sm-$C_A^*(1/3)$ and Sm-$C_A^*(1/2)$, respectively. Although the exact values were not known, q_T's for FI_L and FI_H must be $0<q_T<1/3$ and $1/3<q_T<1/2$, respectively. Note that $q_T=0$ for Sm-C_A^* and $q_T=1$ for Sm-C^*. We will keep using this nomenclature in this paper, because it has been firmly used by recent publications [10–15].

Since then many experimental and theoretical investigations [16–28] clarified step by step the structure of intermediate smectic phases in numerous materials. The sophisti-

*http://polly.phys.msu.ru/~emel/

 ©2010 The American Physical Society

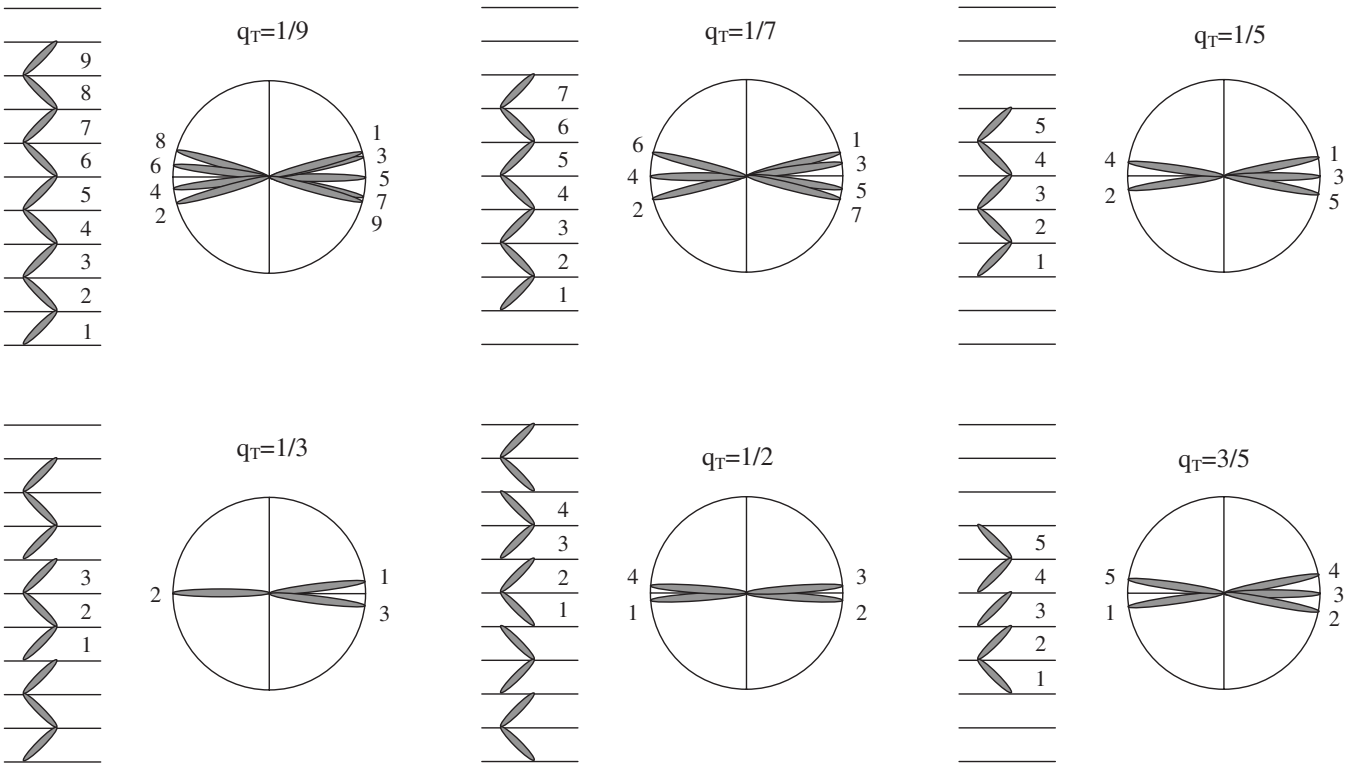

FIG. 1. Biaxial intermediate smectic phases with different numbers of synclinic and anticlinic orderings per period: $q_T=1/9$, 1/7, 1/5, 1/3, 1/2, and 3/5.

cated experimental techniques, such as the polarized resonant x-ray scattering, precision ellipsometry and reflectometry, optical rotatory power, etc., have recently been used to determine the detailed biaxial subphase structures [29–43]. It has been established that Sm-$C_A^*(1/3)$ and Sm-$C_A^*(1/2)$ are, in fact, not coplanar and that the azimuthal angle difference between the directors in the adjacent layers is deviated from $\Delta\varphi=\varphi_i-\varphi_{i-1}=0$ (synclinic) or π (anticlinic). Note that, in these references, Sm-$C_A^*(1/3)$ and Sm-$C_A^*(1/2)$ are designated as FI1 and FI2, respectively. At the same time, the data obtained from ellipsometry studies confirm that three-dimensional (3D) distortion from flat Ising model is not very large [33].

Taking into account all the results mentioned above, in our publications [10,11,44] we were able to derive the molecular-statistical theory predicting the set of possible tilted smectic phases in a particular liquid crystal (LC) material. This theory, however, did not take into account the influence of the electric field on various tilted smectic phases. This problem was investigated on the phenomenological ground, for example, in [23,45–51]. These publications gave considerable contribution into our knowledge about the behavior of smectic phases in the electric field. However, the *magnitude* of the local polarization was considered in these publications to be independent of the tilt planes distribution and generally of the phase type. For example, in Sm-C^* it was considered to be the same as in Sm-C_A^*. In fact, it should be several times smaller, because ferroelectric ordering of polarizations is not favorable, in contrast to antiferroelectric one.

The description of the helix unwinding in liquid crystal phases started from cholesteric phase [52] and was generalized for Sm-C^* in [53–60]. Here, we should mention, however, that in many publications concerning the helix unwinding in smectics only *spontaneous* polarization was taken into account. In many respects it was enough to describe qualitatively the helix unwinding in Sm-C^*. More general theory takes into account both spontaneous and induced polarizations [53] and also describes the influence of surface anchoring on the helix [56]. It is important to note that induced polarization must not solely originate from anisotropy of polarizability of molecules (which is usually assumed in the phenomenological approached to be responsible for *dielectric* effect), but can rather originate from anisotropy of coupling of *permanent* molecular dipole moments in the neighboring smectic layers in the presence of electric field. To distinguish this effect, we are going to call it *dielectriclike* effect. This effect was considered for the first time in [12] in the framework of molecular-statistical approach, and it was shown that its strength can be comparable with that of piezoelectric effect. In particular, we claim that spontaneous polarization does not cause the electric-field-induced transitions from Sm-C_A^* and from biaxial intermediate phases into Sm-C^*, while the anisotropy of coupling of induced polarizations causes these transitions. Our approach also predicts that modification of Sm-C^* itself in the electric field can exhibit two thresholds, which is confirmed experimentally [35,61–65].

It is also important to mention that in [55] an alternative scenario of evolution of Sm-C^* in the electric field was suggested, when the pitch remains constant until the critical electric field is reached, which is due to the formation of stable disclination lines. This type of behavior has been ob-

served experimentally, for example, in [59], and seems to be typical for long-pitch materials (with pitch equal to several micrometers). At the same time, our own spectroscopy measurements in homeotropic samples (unpublished) show that we can easily obtain continuous divergence of the helical pitch at least in the short-pitch smectic materials (with pitch in visible selective reflection range).

In Sec. II we are going to start from the description of polarization effects in various tilted smectic phases. In Sec. III the helix unwinding by the electric field in an arbitrary tilted smectic phase will be considered. The phase sequences in tilted smectic materials and the electric field–temperature phase diagram will be considered in Sec. IV. Finally, in Sec. V the conclusions will be made.

II. POLARIZATION EFFECTS IN VARIOUS TILTED SMECTIC PHASES

We are going to start from the description of polarization effects in various tilted smectic phases (Sm-C^*, Sm-C_A^*, and biaxial intermediate phases), because they are of prime importance for the formation of complex smectic structures and also for the evolution of each particular phase in the electric field. Molecules participating in complex smectic phases usually possess permanent transverse dipole moments located in molecular tails. According to the results obtained in [12], polarization-dependent part of the free energy per smectic layer can be written in the following form:

$$\beta\mu F_{\mathbf{p}}^{(i)} = \mathbf{M}_i \cdot \mathbf{P}_i + \rho\mu\mathbf{M}_i^2, \tag{1}$$

where ρ is the surface density of molecules in smectic layers, μ is the value of molecular transverse terminal dipole moment, $\beta \equiv (k_B T)^{-1}$, k_B is the Boltzmann constant, T is the absolute temperature, and the order parameter $\mathbf{M}_i$ is given by the following expression:

$$\mathbf{M}_i \equiv c_p[\mathbf{n}_i \times \mathbf{k}] + c_f[\mathbf{n}_i \times [\Delta\mathbf{n}_{i\pm1} \times \mathbf{n}_i]] - \beta\mu[\mathbf{n}_i \times [\mathbf{E} \times \mathbf{n}_i]]/4, \tag{2}$$

where $\mathbf{E}$ is the external electric field; $\mathbf{k}$ is the smectic layer normal; $\mathbf{n}_i$ is the nematic director in layer i; parameters c_p and c_f are the piezoelectric and flexoelectric constants, respectively; and the set of polarization vectors is determined by the following equations:

$$\mathbf{P}_i + \hat{\mathbf{g}}[\mathbf{P}_{i-1} + \mathbf{P}_{i+1}] = -\rho\mu\hat{\boldsymbol{\chi}}\mathbf{M}_i, \tag{3}$$

where $\hat{\boldsymbol{\chi}}$ is the dielectric susceptibility tensor for a single smectic layer and $\hat{\mathbf{g}}$ is the dipolar coupling tensor describing the coupling of polarizations in the neighboring smectic layers. Equation (3) represents the three-diagonal set of equations for polarizations, which can be solved explicitly for any given periodicity of the unit cell t, which is different for various tilted smectic phases. However, the solution can be written in the following general form:

$$\mathbf{P}_i = -\rho\mu\sum_{k=0}^{t-1} \hat{\boldsymbol{\omega}}_k \mathbf{M}_{i+k}, \tag{4}$$

where the sum represents residual dielectric effect of the whole set of smectic layers within the unit cell of particular phase, and each dielectric tensor $\hat{\boldsymbol{\omega}}_k$ is the product of diagonal tensors $\hat{\boldsymbol{\chi}}$ and $\hat{\mathbf{f}}_k$ (see [12]). Here, tensor $\hat{\mathbf{f}}_k$ describes the effective long-range interaction due to sequent coupling of polarizations in the neighboring layers only. Substituting Eq. (4) into Eq. (1) and summarizing the free energies of all layers within a unit cell of the phase, one obtains the following expression for polarization-dependent free energy per unit cell:

$$F_{\mathbf{p}} = -\rho k_B T \sum_{i,j=0}^{t-1} (\hat{\boldsymbol{\omega}}_{j-i} - \delta_{ij})\mathbf{M}_i \cdot \mathbf{M}_j. \tag{5}$$

In particular, in Sm-C^*, where the unit cell consists of only one smectic layer, the residual dielectric tensor is the same in every layer. From Eqs. (4) and (5) one readily obtains for polarization and polarization-dependent free energy in Sm-C^*, respectively,

$$\mathbf{P}_i = -\rho\mu\hat{\boldsymbol{\omega}}\mathbf{M}_i, \tag{6}$$

$$F_{\mathbf{p}} = -\rho k_B T(\hat{\boldsymbol{\omega}} - 1)\mathbf{M}_i^2, \tag{7}$$

where $\hat{\boldsymbol{\omega}}$ is the residual dielectric susceptibility tensor taking into account the dipolar coupling in the neighboring smectic layers, whose components along the smectic layer plane and along the smectic layer normal, according to Eq. (3), are equal to

$$\omega_{\parallel} = \frac{\chi_{\parallel}}{1 + 2g_{\parallel}}, \quad \omega_{\perp} = \frac{\chi_{\perp}}{1 + 2g_{\perp}}. \tag{8}$$

According to Eq. (6), the first two terms from Eq. (2) contribute into the spontaneous polarizations (piezoelectric and flexoelectric ones [27,66–68]), while the third term contributes into the *induced* polarization. Thus, according to Eq. (7) [and, generally, to Eq. (5) for arbitrary tilted smectic phase] the polarization-dependent free energy represents the coupling between various kinds of polarization. In particular, the coupling between induced and spontaneous polarizations promotes the piezoelectric and the flexoelectric effects [69–72], which are both proportional to the first power of E, while the coupling between induced polarizations promotes the dielectriclike effect, which is proportional to the second power of E.

It is well known [and it follows from Eqs. (2) and (4)] that both piezoelectric and flexoelectric effects in any tilted smectic phase, where they exist, favor the orientation of the molecular tilt planes perpendicular to the electric field. At the same time, the dielectriclike effect following from anisotropy of coupling between induced polarizations can promote completely different tendencies. In the manner of traditional physics of dielectrics, let us call the dielectriclike effect positive, if it promotes orientation of the tilt planes along the electric field, and negative, if it promotes orientation of the tilt planes perpendicular to the electric field.

In [11,12] it was shown that $g_{\parallel}$ is positive, so that residual dielectric susceptibility within the smectic layer plane $\omega_{\parallel}$ in Sm-C^* is smaller than initial dielectric susceptibility of separate layer $\chi_{\parallel}$ [see Eq. (8)]. This happens due to ferroelectric "side-by-side" coupling of polarizations in the neighboring

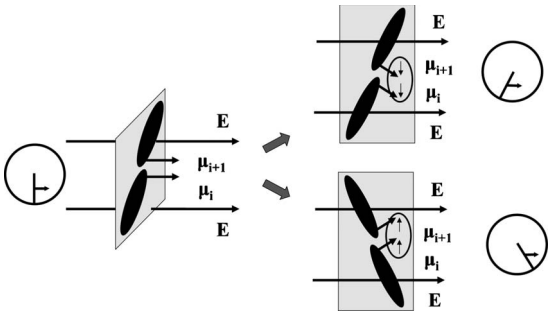

FIG. 2. Qualitative explanation of the tilt plane reorientation in the electric field ($\boldsymbol{\mu}_i$ is the transverse terminal dipole moment of a molecule in layer i). The circular insets show the view of tilt planes and dipole moments from above.

smectic layer planes, which is not favorable. On the contrary, $g_\perp$ is negative, so that residual dielectric susceptibility along the smectic layer normal $\omega_\perp$ in Sm-C^* is larger than initial dielectric susceptibility of separate layer $\chi_\perp$, because ferroelectric "head-and-tail" coupling of polarizations in the neighboring layers along the smectic layer normal is favorable. Thus, the dielectriclike effect will promote those orientations of the molecular tilt planes in Sm-C^*, which reduce the induced polarizations along the smectic layer planes and/or enlarge the induced polarizations along the smectic layer normal. It was shown in [12] that, if the tilt plane has a contribution along or against the electric field direction, then the induced polarization has a contribution along the smectic layer normal (see Fig. 2). Thus, dielectriclike effect in Sm-C^* is positive (promotes the orientation of molecular tilt planes along the electric field).

The situation in other tilted smectic phases is more complicated, because longitudinal and normal to smectic layer plane projections of induced polarizations can form complex sequences from layer to layer. In particular, in Sm-C_A^* the spontaneous part of vector $\mathbf{M}_i$ (which is independent of the electric field) is parallel to the smectic layer plane (similar to that in Sm-C^*), but alternates in sign from layer to layer. The induced part of vector $\mathbf{M}_i$ (which depends on the electric field) has both coplanar and normal to the smectic layer plane projections. The normal projection also alternates in sign from layer to layer, while the coplanar projection has the same direction in every smectic layer. Generally we have shown in [12] that the dielectriclike effect is negative (promotes orientation of the molecular tilt planes perpendicular to the electric field) in Sm-C_A^* and in the whole set of biaxial intermediate phases, unlike that in Sm-C^*.

III. UNWINDING OF THE HELIX IN AN ARBITRARY TILTED SMECTIC PHASE

A. Minimization of the free energy

If the unit cell of the phase (which is equal to one smectic layer in Sm-C^*, to two smectic layers in Sm-C_A^*, and to more smectic layers in the biaxial intermediate phases) exhibits some small helical rotation, it can be approximated with the derivative of local azimuthal orientation φ of the unit cell with respect to coordinate z along the smectic layer normal.

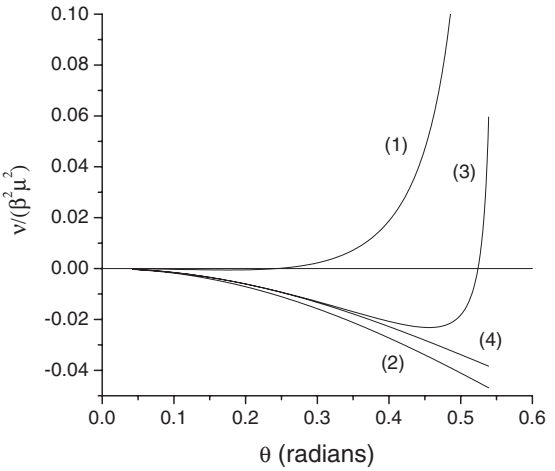

FIG. 3. Anisotropy of coupling between the induced polarizations in neighboring smectic layers as a function of the tilt angle, calculated in the framework of molecular-statistical approach [12] in (1) Sm-C^*, (2) Sm-C_A^*, (3) Sm-$C_A^*(1/3)$, and (4) Sm-$C_A^*(1/2)$.

Then one can write the free energy of an arbitrary tilted smectic phase in the following form:

$$F = f_0 + \frac{1}{2}K\left(\frac{\partial\varphi}{\partial z} - q_0\right)^2 - \lambda E\cos\varphi - \nu E^2\sin^2\varphi, \quad (9)$$

where f_0 is the free energy of the unwound structure of particular phase (which is independent of the helical rotation and orientation of the sample), K is the twist elasticity constant, q_0 is the equilibrium helical wave number at $E=0$, parameter λ determines an influence of the electric field on the spontaneous polarization, and parameter ν determines the dielectriclike effect resulting from anisotropy of coupling between induced polarizations in the neighboring smectic layers discussed in Sec. II. The dependencies of parameter ν on the tilt angle in various smectic phases calculated in the framework of molecular model suggested in [11,12] are presented in Fig. 3. Note that in [12] analogous parameter ν was introduced with the opposite sign. Parameter ν is mostly positive in Sm-C^* (except for very small tilt angles), while it is negative in Sm-C_A^* and in biaxial intermediate phases. It was also discussed in Sec. II that parameter λ is positive in Sm-C^* and in some biaxial intermediate phases [such as Sm-$C_A^*(1/3)$], while it is equal to zero in Sm-C_A^* and in some other biaxial intermediate phases [such as Sm-$C_A^*(1/2)$] where the average spontaneous polarization per each unit cell is equal to zero.

Assuming that at a given value of electric field E the helical smectic structure has a period p, one obtains that the total free energy per pitch is equal to $\mathcal{F} \equiv \int_0^p F(\varphi, \partial\varphi/\partial z)dz$, where functional $F(\varphi, \partial\varphi/\partial z)$ is determined by Eq. (9). The variation of functional $\mathcal{F}$ gives (see Appendix A)

$$\frac{1}{2}\frac{K}{|\nu|E^2}\left(\frac{\partial\varphi}{\partial z}\right)^2 + \frac{\lambda}{|\nu|E}\cos\varphi \pm \sin^2\varphi = \frac{1}{k^2}, \quad (10)$$

where the plus sign must be taken in the case of positive ν, the minus sign must be taken in the case of negative ν, and parameter k must be obtained by minimization of the reduced

free energy $f \equiv 1/p\int_0^p F(\varphi, \partial\varphi/\partial z)dz$. From Eq. (10) it follows that

$$\frac{\partial\varphi}{\partial z} = \frac{\tau q_0}{k}\sqrt{1 - k_0^2\cos\varphi \mp k^2\sin^2\varphi}, \tag{11}$$

where the z-axis direction is chosen for $\partial\varphi/\partial z$ to be positive, $\tau \equiv E\sqrt{2|\nu|/K}/q_0$ is the reduced electric field, $k_0 \equiv ks/\sqrt{\tau}$, and parameter s is defined as follows:

$$s^4 = \frac{2}{Kq_0^2}\frac{\lambda^2}{|\nu|}. \tag{12}$$

Equation (10) can be easily resolved for $\varphi(z)$ provided that we know $k(\tau)$. Substituting Eqs. (10) and (11) into Eq. (9) and integrating the latter with respect to coordinate z from zero to p, one obtains (see Appendix B)

$$\frac{1}{\rho k_B T}\int_0^p F(\varphi, \partial\varphi/\partial z)dz = pf_0 - 2\pi Kq_0 + \frac{K\tau q_0}{2k}\{2G_2(k,\tau) - G_1(k,\tau)\}, \tag{13}$$

where

$$G_1(k,\tau) \equiv \int_0^{2\pi}\frac{1}{\sqrt{1 - k_0^2\cos\varphi \mp k^2\sin^2\varphi}}d\varphi,$$

$$G_2(k,\tau) \equiv \int_0^{2\pi}\sqrt{(1 - k_0^2\cos\varphi \mp k^2\sin^2\varphi)}d\varphi. \tag{14}$$

From Eq. (11) it also follows that

$$p \equiv \int_0^{2\pi}\left(\frac{\partial\varphi}{\partial z}\right)^{-1}d\varphi = \frac{k}{\tau q_0}G_1(k,\tau). \tag{15}$$

Dividing Eq. (13) by Eq. (15), one obtains for the reduced free energy

$$\frac{f}{\rho k_B T} = f_0 + \frac{1}{2}Kq_0^2\tau^2\left\{-\frac{1}{k^2} + \frac{2}{kG_1}\left(\frac{G_2}{k} - \frac{2\pi}{\tau}\right)\right\}. \tag{16}$$

Minimizing f with respect to k (see Appendix C), one obtains the following equation for determination of k:

$$\frac{G_2(k,\tau)}{k} = \frac{2\pi}{\tau}. \tag{17}$$

The expression for the equilibrium free energy can be obtained by substitution of Eq. (17) into Eq. (16):

$$\frac{f}{\rho k_B T} = f_0 - \frac{Kq_0^2\tau^2}{2k^2}. \tag{18}$$

Equation (17) must be solved numerically for k at every electric field value τ. Parameters k and $k_0 = ks/\sqrt{\tau}$ must be then substituted into Eq. (11), and the latter must be resolved for $\varphi(z)$, so that the helical structure at any electric field value will be obtained. From the definition of parameter s [Eq. (12)] one obtains the following correlation between electric field E and the new reduced electric field τ:

$$\tau = E|\nu|s^2/\lambda, \tag{19}$$

which appears to be the only variable the solution explicitly depends on (at a given parameter s). Since $q_0 = 2\pi/p_0$, where p_0 is the equilibrium helical pitch at $\tau = 0$, from Eqs. (11) and (17) it also follows that

$$p = \frac{1}{4\pi^2}G_1(k)G_2(k)p_0. \tag{20}$$

Parameters k and k_0 and dimensionless helical pitch p/p_0 in the case of positive ν are presented in Figs. 4(a)–4(c), respectively, as functions of the reduced electric field τ. The same dependencies in the case of negative ν are presented in Figs. 5(a)–5(c). One notes that the dependence $p/p_0(\tau)$ is generally similar to that in cholesterics [52,73]. At the same time, it is interesting to investigate the detailed modification of smectic structure in the electric field. The latter essentially depends on the sign of parameter ν and on the value of parameter s, which effectively determines the ratio between the effect of spontaneous polarization and the effect of induced polarization at a given reduced electric field τ. Parameter s [see Eq. (12)] depends only on the material properties and on the tilt angle, so this is a fixed parameter in a particular material at a particular temperature. For each value of parameter s, the helical pitch diverges at particular reduced electric field $\tau = \tau^*$. One notes that at given parameter s the evolution of the unit-cell azimuthal distribution with variation of reduced electric field τ is the same, independent of the phase type (Sm-C^*, Sm-C_A^*, or biaxial intermediate phase). At the same time, the correlation between real electric field E and reduced electric field τ is specific to a particular phase via parameters λ and ν. [see Eq. (19)], and therefore the real unwinding thresholds are generally different in various smectic phases.

B. Case 1: Coupling of induced polarizations in neighboring smectic layers promotes positive dielectriclike effect ($\nu > 0$)

1. General scope

It was discussed in Sec. III A that $\nu > 0$ is the most typical case in Sm-C^*, except for very small tilt angles. In the case of positive ν one must take the minus sign in Eq. (11). To investigate the evolution of helical structure of Sm-C^* in the electric field, one needs to find the roots of equation

$$k^2\cos^2\varphi - k_0^2\cos\varphi + (1 - k^2) = 0, \tag{21}$$

corresponding to expression under the square root in Eq. (11). For this reason one needs to investigate the sign of discriminant

$$D = k_0^4 - 4k^2(1 - k^2). \tag{22}$$

From Eqs. (14) and (17) it follows that k is approximately proportional to τ at small values of the reduced electric field τ. Therefore, $D \to k^2(s^4 - 4)$ at $\tau \to 0$. Thus, $D < 0$ at small electric field if $s < \sqrt{2}$ and $D > 0$ at small electric field if $s > \sqrt{2}$.

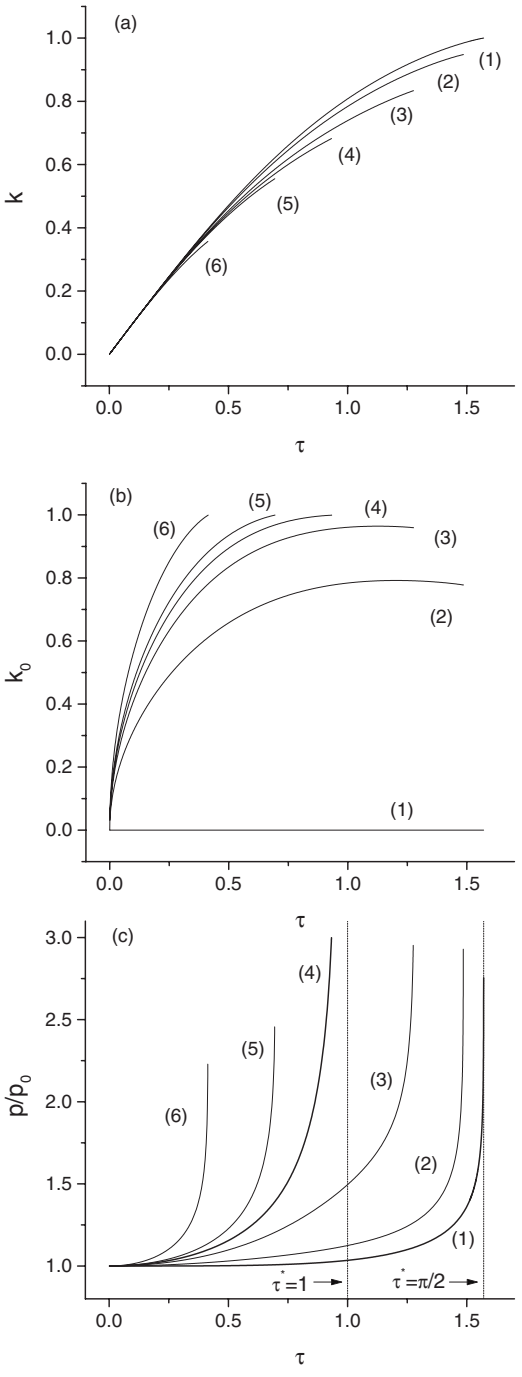

FIG. 4. Parameters (a) k and (b) k_0 and (c) dimensionless helical pitch p/p_0 as functions of reduced electric field τ in the case of positive ν: $s=0$ (1), 1.0 (2), 1.3 (3), $\sqrt{2}$ (4), 1.5 (5), and 1.8 (6).

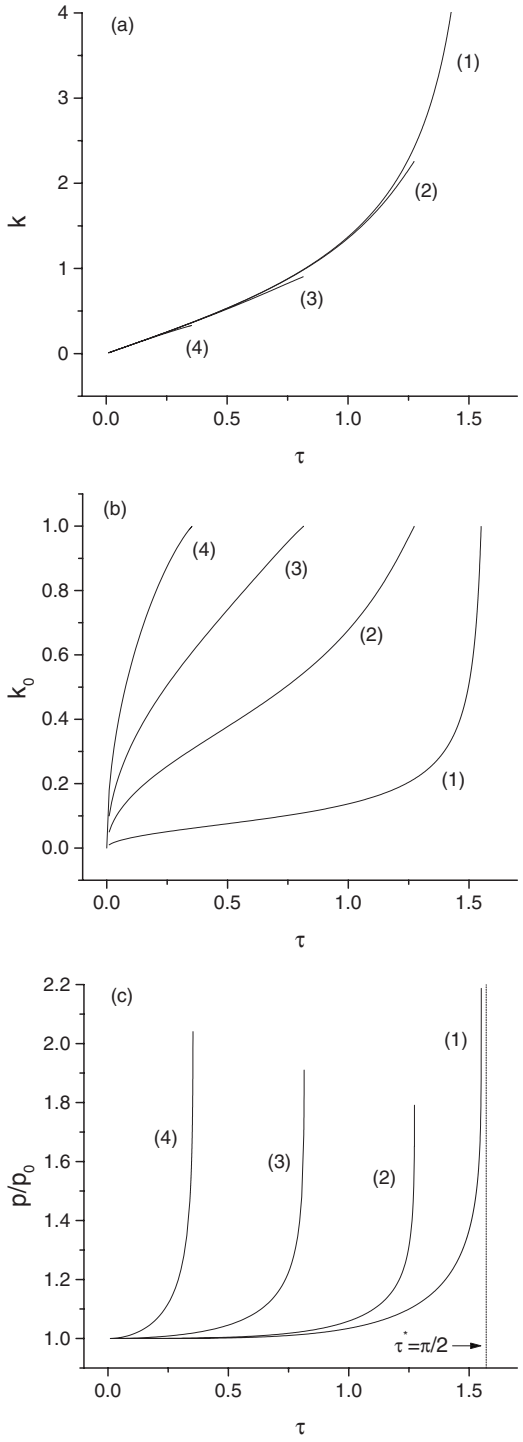

FIG. 5. Parameters (a) k and (b) k_0 and (c) dimensionless helical pitch p/p_0 as functions of reduced electric field τ in the case of negative ν: $s=0.1$ (1), 0.5 (2), 1.0 (3), and 1.8 (4).

2. Case 1(a): Effect of induced polarization is already noticeable before unwinding of the helix ($0<s<\sqrt{2}$)

In this case discriminant (22) is negative at small electric field, Eq. (21) has no roots with respect to cos φ, and the helical pitch is finite. Therefore, the helical pitch must diverge, when Eq. (21) begins to have at least one root with respect to cos φ at cos $\varphi \leq 1$. This happens when discriminant (22) becomes equal to zero. In this case both roots of Eq. (21) become equal to

$$\cos \varphi^* \equiv \frac{\sqrt{1-k^{*2}}}{k^*}, \tag{23}$$

where "star" indicates the critical unwinding values of the corresponding parameters, and integral $G_2(k,\tau)$ [see Eq. (14)] becomes equal to

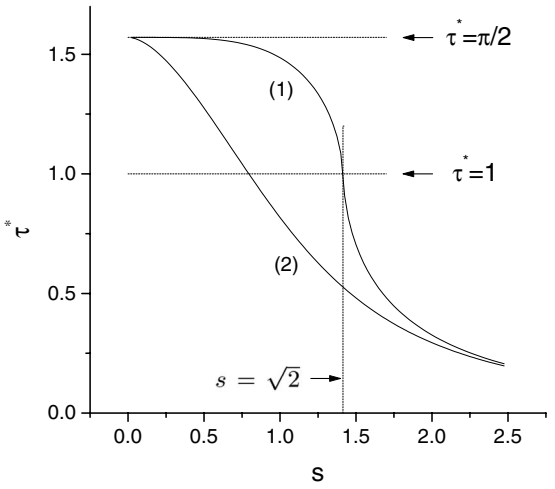

FIG. 6. Critical unwinding reduced electric field as a function of an effective ratio between spontaneous and induced polarization effects in cases (1) $\nu>0$ and (2) $\nu<0$.

$$G_2(k^*,\tau^*) = \int_0^{2\pi} |\sqrt{1-k^{*2}} - k^* \cos\varphi| d\varphi$$
$$= -\int_{-\varphi^*}^{\varphi^*} (\sqrt{1-k^{*2}} - k^* \cos\varphi) d\varphi$$
$$+ \int_{\varphi^*}^{2\pi-\varphi^*} (\sqrt{1-k^{*2}} - k^* \cos\varphi) d\varphi$$
$$= (2\pi - 4\varphi^*)\sqrt{1-k^{*2}} + 4k^* \sin\varphi^*$$
$$= 2k^*\{(\pi - 2\varphi^*)\cos\varphi^* + 2\sin\varphi^*\}, \quad (24)$$

which, according to Eq. (17), should be equal to $2\pi k^*/\tau^*$. On the other hand, from zero discriminant (22) it follows that $k_0^{*2}=2k^*\sqrt{1-k^{*2}}$, which—according to definition Eq. (12)—should be equal to $k^{*2}s^2/\tau^*$. Therefore, at positive ν and $0<s<\sqrt{2}$ the critical unwinding reduced electric field is equal to

$$\tau^* = \frac{s^2}{2\cos\varphi^*}, \quad (25)$$

where angles $\pm\varphi^*$ are the azimuthal orientations of two domains of the unwound bidomain structure at τ^*, since $\cos\varphi^*$ is the root of Eq. (21) and, according to Eq. (11), $\partial\varphi/\partial z=0$ at $\pm\varphi^*$. Combination of Eqs. (24) and (25) yields the following recurrent equation for determination of φ^* at $0<s<\sqrt{2}$:

$$\varphi^* = \tan\varphi^* + \frac{\pi}{2}\left(1 - \frac{2}{s^2}\right). \quad (26)$$

It follows from Eq. (26) that orientation of the tilt planes $\pm\varphi^*$ at divergence of the helical pitch varies between zero and $\pm\pi/2$ depending on the value of parameter s. One notes from Eq. (25) that the value of critical reduced electric field τ^* (as well as φ^*) depends only on the value of parameter s. This dependence in the case $0<s<\sqrt{2}$ is presented in Fig. 6, curve (1), left from the vertical dashed line.

Since $E=\tau\lambda/(s^2|\nu|)$ [see Eq. (19)], then the critical unwinding electric field at $\nu>0$ and $0<s<\sqrt{2}$ is equal to

$$E^* = \frac{\lambda}{2\nu\cos\varphi^*}. \quad (27)$$

In the limit case $s\to 0$ (spontaneous polarization is absent) the solution of Eq. (26) $\varphi^*(s)$ tends to $\pi/2$ (the induced polarization promotes orientation of the tilt planes either along or against the electric field direction at divergence of the helical pitch). In this case Eqs. (25) and (27) become formally not applicable, and the critical unwinding electric field must be obtained directly from Eqs. (17) and (24) at $\varphi^*=\pi/2$, i.e., $\tau^*=\pi/2$, and consequently $E^*=\pi q_0\sqrt{K/(2|\nu|)}/2$.

In the opposite limit case $s\to\sqrt{2}$ (spontaneous polarization is strong and almost suppresses the effect of induced polarization) solution $\varphi^*(s)$ tends to zero (the tilt planes are oriented perpendicular to the electric field at divergence of the helical pitch), τ^* tends to 1 [see Eq. (25)], k^{*2} tends to 0.5 [see Eq. (23)], and k_0 tends to 1 [from zero discriminant (22)].

The view from above on the distribution of tilt planes within one helical pitch at $s=1.3$, which belongs to interval $0<s<\sqrt{2}$, is shown by radial lines in Fig. 7 at several values of the electric field. At zero electric field the distribution is uniform (distances between the neighboring radial lines are the same in every sector of the circle). When the electric field is applied perpendicular to the helical axis, the tilt planes first tend to collect in one semicircle with preference in the direc-

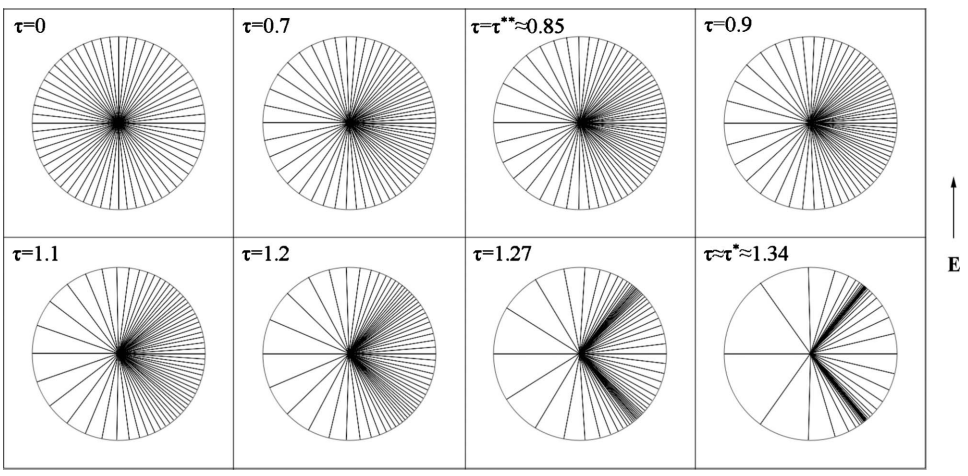

FIG. 7. View from above on the distribution of tilt planes within one helical pitch at $\nu>0$ and $s=1.3$. The local directions of tilt planes are shown by the radial lines with some periodicity along the z axis. A set of snapshots for various reduced electric field values is presented.

tion perpendicular to the electric field due to spontaneous polarization, which prefers to be oriented along the electric field. The term proportional to λ in Eq. (9) is responsible for this tendency. However, starting from some critical value of the reduced electric field τ^{**}, the maximum density of the tilt planes splits into two symmetrical maxima. One of them shifts clockwise, and another one shifts anticlockwise, when the electric field farther increases, so that the bidomain structure arises, where the most of the tilt planes gain contributions either along or against the electric field direction. The term proportional to ν in Eq. (9) is responsible for this tendency. Differentiating Eq. (10) with plus sign (which is in the case of positive ν) with respect to coordinate z, it is easy to obtain that $E^{**}=\lambda/(2\nu)$ and, thus, $\tau^{**}=s^2/2$ [see Eq. (19)]. Below this value the maximum density of the tilt planes corresponds to $\varphi=0$ and minimum corresponds to $\varphi=\pi$, while above τ^{**} the two minima correspond to $\varphi=0$ and $\varphi=\pi$, and the two maxima correspond to $\varphi=\pm\arccos\{\lambda/(2\nu E)\}=\pm\arccos\{s^2/(2\tau)\}$. Before the helical pitch diverges at τ^*, the tilt planes gain more and more contribution either along or against the electric field due to coupling of the induced polarizations in the neighboring layers [12]. From Eq. (25) it follows that $\tau^*>\tau^{**}$ if $0<s<\sqrt{2}$. In other words, the helical bidomain structure arises first, and the helical pitch always diverges at larger values of electric field.

3. Case 1(b): Effect of induced polarization is only noticeable after unwinding of the helix ($s>\sqrt{2}$)

In this case discriminant (22) is always positive, and Eq. (21) has always two roots with respect to $\cos\varphi$. However, one can check that at small values of electric field τ both roots are larger than 1. Therefore, the helical pitch must diverge, when the smaller root of Eq. (21) becomes equal to 1. Therefore, in the case $\nu>0$ and $s>\sqrt{2}$ the tilt planes at helical pitch divergence become perpendicular to the electric field direction ($\varphi^*=0$), and the unwound structure at divergence point is monodomain. It is easy to check that solution $\cos\varphi^*=1$ in the case $s\neq 0$ corresponds to $k_0^*=1$. In this case integral $G_2(k,\tau)$ [see Eq. (14)] becomes equal to

$$G_2(k^*,\tau^*)=\int_0^{2\pi}\sqrt{(1-\cos\varphi)(1-k^{*2}-k^{*2}\cos\varphi)}d\varphi = \frac{1}{k^*}\left[\frac{\pi}{2}-\arcsin(1-4k^{*2})\right]+2\sqrt{2-4k^{*2}}, \tag{28}$$

which, according to Eq. (17), should be equal to $2\pi k^*/\tau^*$. On the other hand, from $k_0^*=1$ it follows that, according to definition (12), the critical unwinding reduced electric field is equal to

$$\tau^*=k^{*2}s^2. \tag{29}$$

One obtains from Eqs. (28) and (29) the following recurrent equation for determination of k^*:

$$k^*=\frac{1}{\sqrt{2}}\sin\left(\frac{\pi}{s^2}-k^*\sqrt{2-4k^{*2}}\right). \tag{30}$$

At $s\to\sqrt{2}$ (on approach from the right), the solution of Eq. (30) k^{*2} tends to 0.5, and τ^* therefore tends to 1 [see Eq. (29)], so that the solution coincides with that on approaching from the left, considered in Sec. III B 2, and dependencies $\tau^*(s)$ and $k^*(s)$ appear to be continuous at $s=\sqrt{2}$. The continuation of dependence of the critical reduced electric field τ^* on parameter s in the case $s\geq\sqrt{2}$ is presented in Fig. 6, curve (1), right from the vertical dashed line.

Since $E=\tau\lambda/(s^2|\nu|)$ [see Eq. (19)], then the critical electric field at $\nu>0$ and $s\geq\sqrt{2}$ is equal to

$$E^*=\frac{\lambda k^{*2}}{|\nu|}, \tag{31}$$

where k^* is the root of Eq. (30). By analogy to case 1(a) considered in Sec. III B 2, let us introduce another critical electric field value $E^{**}=\lambda/(2\nu)$, at which the tilt planes gain some contribution either along or against the electric field. From the solution of Eq. (30) it follows that $k^{*2}\leq 0.5$ in the case $\nu>0$ and $s\geq\sqrt{2}$, and thus from Eq. (31), $E^*\leq E^{**}$, just opposite to the case $0<s<\sqrt{2}$. In other words, the helical pitch diverges first, and the bidomain structure can only arise at larger values of the electric field. This process will be considered separately in Sec. III B 4.

The view from above on the distribution of tilt planes within one helical pitch at $s=1.5$, which belongs to interval $s>\sqrt{2}$, is shown by radial lines in Fig. 8, first row, at several values of the electric field. One notes that the tilt planes tend to collect in one semicircle with preference in the direction, perpendicular to the electric field due to spontaneous polarization, while the induced polarization has no any noticeable effect until $\tau^{**}=s^2/2$, and thus the tilt plane of the unwound structure stays perpendicular to the electric field within the interval $\tau^*<\tau\leq\tau^{**}$.

4. Bidomain smectic structures after unwinding: Solitary waves

In the previous two sections we considered separately a modification of the helical smectic structure in two cases: $0<s<\sqrt{2}$ and $s\geq\sqrt{2}$. In the case $0<s<\sqrt{2}$ the bidomain helical structure takes place with two most probable azimuthal orientations $\pm\varphi\neq 0$ of the tilt planes. The question arises of how these two domains coexist after the helical pitch divergence. In the case $s\geq\sqrt{2}$ the helical structure is always monodomain (there is only one most probable azimuthal orientation $\varphi=0$); but, nevertheless, at larger values of the electric field (at $\tau>\tau^{**}$), still the two possibilities of the azimuthal orientation arise, and the question is the same: how do these two possibilities coexist?

It was discussed in Sec. III B 2 that in the case $0<s<\sqrt{2}$ the helical pitch diverges when discriminant (22) becomes equal to zero (being initially negative). In contrast, in Sec. III B 3 it was discussed that in the case $s\geq\sqrt{2}$ discriminant (22) is initially positive, but both roots of Eq. (21) with respect to $\cos\varphi$ are initially larger than 1, and thus the helical pitch diverges when the lower root becomes equal to 1.

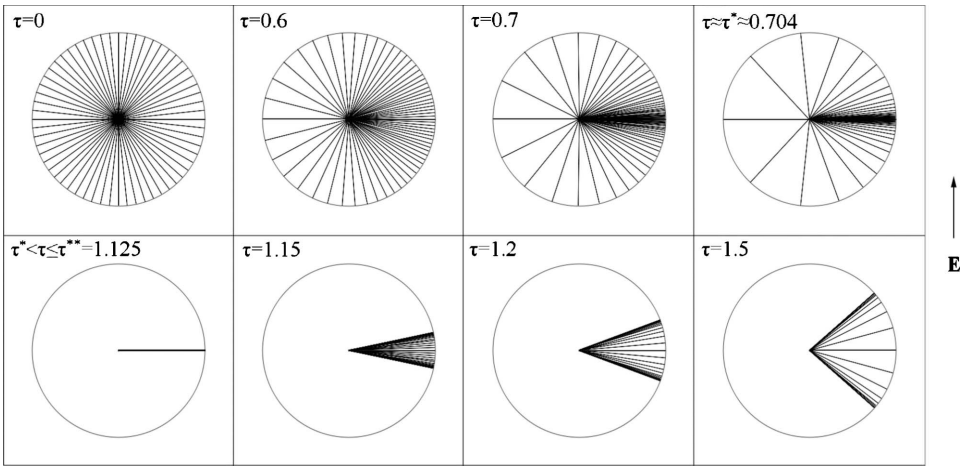

FIG. 8. View from above on the distribution of tilt planes within one helical pitch at $\nu>0$ and $s=1.5$. The local directions of tilt planes are shown by the radial lines with some periodicity along the z axis. A set of snapshots for various reduced electric field values is presented.

In both cases $0<s<\sqrt{2}$ and $s\geq\sqrt{2}$ Eq. (17) [that was used for determination of parameter $k(\tau)$ in the helical state] has no solutions at $\tau>\tau^*$ (i.e., at the electric field exceeding the critical unwinding value) anymore, and the minimum free energy (16) with respect to parameter k simply corresponds to the edge of the definition range of real parameter k. In the case $0<s<\sqrt{2}$ this edge is a prolongation of the critical constraint at the unwinding point, i.e., $D=0$. In the case $s\geq\sqrt{2}$ a prolongation of the critical constraint is $k_0=1$ promoting the lower root of Eq. (21) with respect to cos φ to be equal to 1. Equation (11) in this case has only one solution, $\varphi=\text{const}=0$. However, at $\tau^{**}=s^2/2$ both roots of Eq. (21) with respect to cos φ become equal to each other, and starting from τ^{**} the edge of the definition range of real parameter k becomes $D=0$, similarly to the case $0<s<\sqrt{2}$. Thus, the question of coexistence of two domains after the unwinding (which is actual at the reduced electric field larger than both τ^* and τ^{**}, independent of their relative values) can be generalized for both cases $0<s<\sqrt{2}$ and $s\geq\sqrt{2}$.

The constraint $D=0$ yields $k_0^2=2k\sqrt{1-k^2}$ [see Eq. (22)], which—on the other hand—should be equal to k^2s^2/τ, and therefore one obtains the following dependence at $\tau>\max\{\tau^*,\tau^{**}\}$:

$$k(\tau)=\frac{2\tau}{\sqrt{s^4+4\tau^2}}. \tag{32}$$

In this case Eq. (11) can be rewritten (taking into account the constraint $D=0$) as follows:

$$\frac{\partial\varphi}{\partial z}=\frac{\tau q_0}{k}\left|\sqrt{1-k^2}-k\cos\varphi\right|. \tag{33}$$

One notes that two trivial solutions of Eq. (33) corresponding to the minimum free energy (stable equilibrium) are $\pm\varphi_0$, where $\varphi_0\equiv\arccos\sqrt{1-k^2}/k$. However, the coexistence of two domains is described by a different (nontrivial) solution of Eq. (33) corresponding to the maximum free energy (nonstable equilibrium):

$$\varphi=\pm 2\arctan\left\{\tan\frac{\varphi_0}{2}\tanh^{\pm 1}\left[\frac{1}{2\tau}q_0(z-z_i)\sin\varphi_0\right]\right\}, \tag{34}$$

where z_i is the limited number of points along the smectic layer normal, where the domain walls [53,74,75] are located, the plus sign must be taken at $2\pi n-\varphi_0<\varphi<2\pi n+\varphi_0$, the minus sign must be taken at $2\pi n+\varphi_0<\varphi<2\pi(n+1)-\varphi_0$, and n is an arbitrary integer number. Solution (34) formally corresponds to a conjugation of two opposite infinite domains. However, really the length of each domain is determined by prehistory of their creation at bifurcation point ($\tau=\tau^*$ at $0<s<\sqrt{2}$ or $\tau=\tau^{**}$ at $s\geq\sqrt{2}$).

A possible (helical) conjugation is presented in Fig. 9. This type of conjugation will most likely take place in the case $0<s<\sqrt{2}$, when two finite domains already exist within the deformed helical structure, and will most likely continue to exist in a helixlike form after divergence of the helical pitch, coinciding with bifurcation point at $0<s<\sqrt{2}$.

Another (oscillating) type of conjugation (see Fig. 10) can take place in the case $s\geq\sqrt{2}$, when the helical pitch diverges

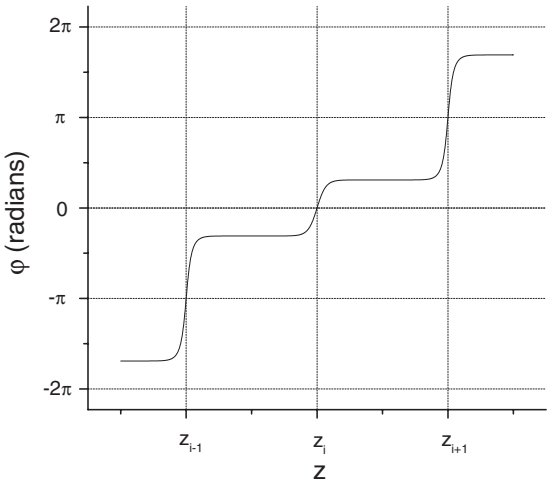

FIG. 9. An example of helical conjugation of domains according to Eq. (34) in case $\nu>0$, $0<s<\sqrt{2}$, and $\tau>\tau^*>\tau^{**}$: $s=1.3$ (the same as in Fig. 7) and $\tau=1.5$. Here, z_i are some conjugation points.

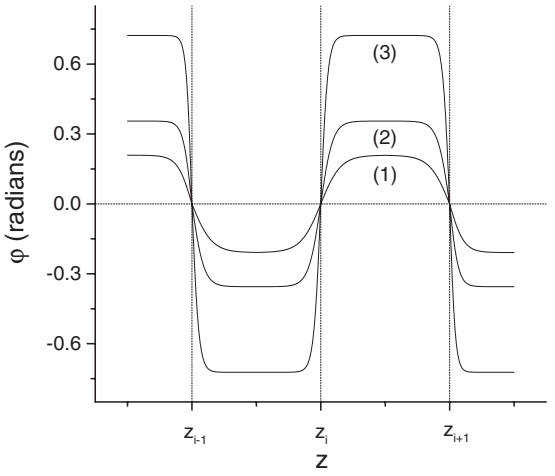

FIG. 10. An example of oscillating conjugation of domains according to Eq. (34) in case $\nu>0$, $s>\sqrt{2}$, and $\tau>\tau^{**}>\tau^{*}$: $s=1.5$ (the same as in Fig. 8) and $\tau=1.15$ (1), 1.2 (2), and 1.5 (3). Here, z_i are some conjugation points.

within the monodomain helical structure long before the bifurcation point, so that bifurcation arises in a single domain with $\varphi=0$. This conjugation can be obtained if one generalizes Eq. (33) for the case of symmetrical negative derivative that was ignored in the original Eq. (11), because it did not match the minimum free energy.

The corresponding smectic structure evolution in the electric field exceeding $\tau^{**}=s^2/2$ (the view from above on the distribution of tilt planes within one solitary wave at $s=1.5$) is shown by radial lines in Fig. 8, second row. Starting from τ^{**} the maximum density of the tilt planes splits into two symmetrical maxima. One of them shifts clockwise (and tends to $\pi/2$ at $\tau\to\infty$), while another one shifts anticlockwise (and tends to $-\pi/2$ at $\tau\to\infty$).

C. Case 2: Coupling of induced polarizations in neighboring smectic layers promotes negative dielectriclike effect ($\nu<0$)

It was discussed in Sec. III A that $\nu<0$ is typical for Sm-C_A^* and for biaxial intermediate phases. In the case of negative ν one must take the plus sign in Eq. (11). To investigate the evolution of helical structure of these phases in the electric field, one needs to find the roots of equation

$$-k^2\cos^2\varphi - k_0^2\cos\varphi + (1+k^2) = 0, \tag{35}$$

corresponding to expression under the square root in Eq. (11). Dissimilar to the case considered in Sec. III B, the discriminant

$$D = k_0^4 + 4k^2(1+k^2) \tag{36}$$

is always positive, and Eq. (35) has always two roots with respect to $\cos\varphi$. However, one can check that at small values of the electric field τ both roots are larger than 1. Therefore, the helical pitch must diverge, when the smaller root of Eq. (35) becomes equal to 1. Therefore, at negative ν the unwound structure of Sm-C^* is monodomain with $\varphi^*=0$ (the tilt plane is perpendicular to the electric field direction). It is easy to check that solution $\cos\varphi^*=1$ in the case $s\neq 0$ corresponds to $k_0^*=1$. In this case integral $G_2(k,\tau)$ [see Eq. (14)] becomes equal to

$$G_2(k^*,\tau^*) = \int_0^{2\pi}\sqrt{(1-\cos\varphi)(1+k^{*2}+k^{*2}\cos\varphi)}d\varphi$$
$$= \frac{1}{k^*}\ln[1+4k^{*2}+2k^*\sqrt{2(1+2k^{*2})}]$$
$$+ 2\sqrt{2(1+2k^{*2})}, \tag{37}$$

which, according to Eq. (17), should be equal to $2\pi k^*/\tau^*$. Similarly to the case considered in Sec. III B 3, from $k_0^*=1$ it follows that, according to definition (12), the critical unwinding reduced electric field is determined by Eq. (29). Introducing a new parameter $x\equiv k\sqrt{2(1+2k^2)}$, one obtains from Eqs. (37) and (29) the following recurrent equation for determination of x^*:

$$x^* = \frac{\pi}{s^2} - \frac{1}{2}\ln[2x^* + \sqrt{1+4x^{*2}}]. \tag{38}$$

At $s\to 0$ solution $x^*(s)$ tends to infinity, while at $s\to\infty$ it tends to zero. From x one can easily change to k according to definition of x:

$$k^* = \tfrac{1}{2}\{(1+4x^{*2})^{1/2}-1\}^{1/2}, \tag{39}$$

and then one obtains τ^* from Eq. (29). The corresponding dependence of the critical reduced electric field τ^* on parameter s is presented in Fig. 6, curve (2). From Eq. (19) it follows that the critical electric field E^* at $\nu<0$ and $s\neq 0$ is determined by Eq. (31) obtained in Sec. III B 3 for the case $\nu>0$ and $s>\sqrt{2}$, where k^*, however, is determined by Eq. (39), where x^* is the solution of Eq. (38).

In particular, the view from above on the distribution of unit-cell azimuthal orientations within one helical pitch in Sm-$C_A^*(1/3)$ (intermediate biaxial phase with the three-layer unit cell, which is also called FI1 in the literature) is presented in Fig. 11 for several values of reduced electric field τ. The radial lines show the average tilt direction per unit cell. At zero electric field the distribution is uniform (the unit cells rotate uniformly). When the electric field is applied perpendicular to the helix axis, the tilt planes tend to collect perpendicular to the electric field. In the same manner, as in Sm-C^* at $s>\sqrt{2}$, the unit cells in Sm-$C_A^*(1/3)$ exhibit a distortion in the electric field in a polar way, because the average spontaneous polarization is not equal to zero.

In Sm-C_A^* and in Sm-$C_A^*(1/2)$ (intermediate biaxial phase with the four-layer unit cell, which is also called FI2 in the literature) the average spontaneous polarization per unit cell is equal to zero, and therefore $s=0$. In this case Eq. (11) for determination of $\varphi(z)$ can be rewritten as

$$\frac{\partial\varphi}{\partial z} = \frac{\tau q_0}{k}\sqrt{1+k^2\sin^2\varphi}, \tag{40}$$

where parameter k must be obtained from Eq. (17). One also notes that integrals G_1 and G_2 [see Eq. (14)] in the case $k_0=0$ (following from $\lambda=0$) become independent of electric field τ.

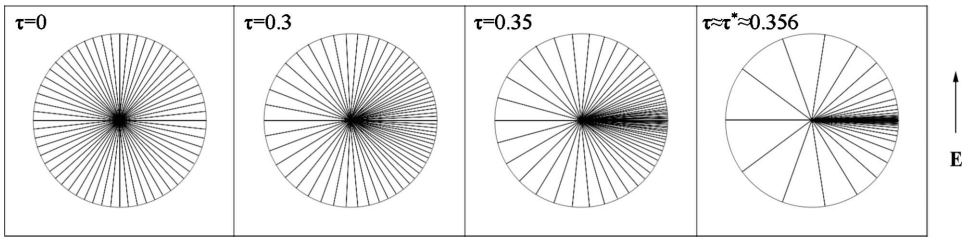

FIG. 11. View from above on the distribution of local three-layer unit cells in Sm-$C_A^*(1/3)$ within one helical pitch ($\nu<0$ and $s=1.8$). Each radial line represents the average orientation of the tilt planes within particular three-layer unit cell. These orientations are shown with some periodicity along the z axis. A set of snapshots for various reduced electric field values is presented.

$$G_1(k) \equiv \int_0^{2\pi} \frac{1}{\sqrt{1+k^2\sin^2\varphi}} d\varphi,$$

$$G_2(k) \equiv \int_0^{2\pi} \sqrt{1+k^2\sin^2\varphi}\, d\varphi. \tag{41}$$

Solution $\varphi(z)$ following from Eq. (40) describes the distribution of unit-cell azimuthal orientation along the smectic layer normal z at a given value of the electric field E. At $s=0$ Eqs. (29) and (31) become formally not applicable, because Eq. (35) at $k_0=0$ has two roots $\cos\varphi^*=\pm\sqrt{1+1/k^2}$, and one of them becomes equal to 1 only at $k^*\to\infty$. In this case integral $G_2(k,\tau)$ tends to

$$G_2(k^*,\tau^*) \to k^* \int_0^{2\pi} \sqrt{1-\cos^2\varphi}\, d\varphi = 4k^*, \tag{42}$$

which, according to Eq. (17), should be equal to $2\pi k^*/\tau^*$. From here one concludes that $\tau^*=\pi/2$, and consequently $E^*=\pi q_0\sqrt{K/(2|\nu|)}/2$. These results coincide with the limits of Eqs. (29) and (31) at $s\to 0$. One notes that the critical unwinding electric field in the case $s=0$ does not depend on the sign of parameter ν, i.e., it is exactly the same as was obtained in Sec. III B 2. This result can be understood already from free energy (9) at $\lambda=0$ (that follows from $s=0$). Indeed, if $\lambda=0$, then one can change over from φ to $\pi/2-\varphi$ and simultaneously from ν to $-\nu$, and two cases considered here and in Sec. III B become formally nondistinguishable [see Fig. 6]. One can also see from Fig. 6 that solutions at $\nu<0$ and $\nu>0$ tend to each other at $s\to\infty$ (i.e., when $|\nu|\to 0$).

The view from above on the distribution of unit-cell azimuthal orientation within one helical pitch in Sm-C_A^* and in Sm-$C_A^*(1/2)$ is presented in Fig. 12 for several values of reduced electric field $\tau=E\sqrt{2|\nu|/K}/q_0$. At zero electric field the distribution is uniform (the unit cells rotate uniformly). When the electric field is applied perpendicular to the helix axis, the tilt planes always tend to collect perpendicular to the electric field due to coupling of the induced polarizations in neighboring layers. Dissimilar to that in Sm-C^* and in Sm-$C_A^*(1/3)$, the unit cells in Sm-C_A^* and in Sm-$C_A^*(1/2)$ exhibit a distortion in the electric field in a nonpolar way.

One notes that for any value of s at $\nu<0$ the monodomain helical structure is unwound at E^*, and the monodomain flat structure with the tilt plane perpendicular to the electric field arises. In contrast to the case $\nu>0$ considered in Sec. III B, both helical and unwound bidomain structures are not possible at $\nu<0$.

IV. PHASE SEQUENCES IN TILTED SMECTIC MATERIALS AND ELECTRIC FIELD–TEMPERATURE PHASE DIAGRAM

The general expression for the free energy F of an arbitrary tilted smectic phase per smectic layer including both polarization-dependent part discussed in Sec. II and polarization-independent part discussed in [11] can be written in the following way:

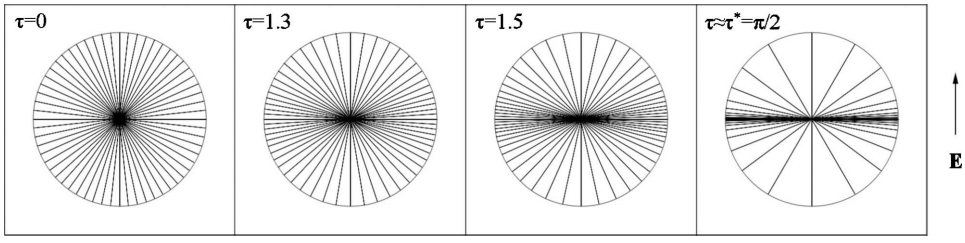

FIG. 12. View from above on the distribution of local unit cells in Sm-C_A^* and in Sm-$C_A^*(1/2)$ within one helical pitch ($\nu<0$ and $s=0$). Each radial line represents the average orientation of the tilt planes within particular two- or four-layer unit cell. These orientations are shown with some periodicity along the z axis. A set of snapshots for various reduced electric field values is presented.

$$\frac{t[F-F_0(\theta)]}{\rho k_B T}=\left(\frac{3}{2}v_1-g_1^2+4c_f^2\right)\sum_{i=0}^{t-1}(\mathbf{n}_i\cdot\mathbf{n}_{i+1})^2+(v_3+6g_1^2)\cos^2\theta\sum_{i=0}^{t-1}(\mathbf{n}_i\cdot\mathbf{n}_{i+1})+v_5\sum_{i=0}^{t-1}(\mathbf{n}_i\cdot\mathbf{n}_{i+1})(\mathbf{k}\cdot[\mathbf{n}_i\times\mathbf{n}_{i+1}])-\sum_{i,j=0}^{t-1}(\hat{\boldsymbol{\omega}}_{|j-i|}-\delta_{ij})\mathbf{M}_i\cdot\mathbf{M}_j, \quad (43)$$

where $F_0(\theta)$ is the free energy related to the interaction of molecules within their smectic layers only. The first three terms in Eq. (43) represent the polarization-independent interactions between molecules located in the neighboring smectic layer [where terms proportional to coefficients v_1 and v_3 describe nonchiral dispersion interactions, the term proportional to v_5 describes chiral dispersion interaction, terms proportional to g_1^2 represent the dipole-dipole interaction treated in the second virial expansion, and the term proportional to c_f^2 represents the dipole-quadrupole interaction treated in the second virial expansion (in the latter two kinds of terms only *transverse* molecular dipoles participate)], while the fourth term is the effective long-range interaction arising due to coupling of polarizations in the neighboring smectic layers. For simplicity the electrostatic interactions arising due to *longitudinal* molecular dipoles, as well as quadrupole-quadrupole and higher multipole interactions between molecules located in the neighboring smectic layers, are included into terms proportional to v_1 and v_3, which are known as *quadrupolar* and *dipolar* terms, respectively, having mostly dispersion origin.

The physical (or geometrical) meaning of the first tree terms in Eq. (43) can easily be understood if one rewrites them in terms of tilt angle θ (which is assumed to be the same in every smectic layer) and azimuthal rotation $\Delta\varphi$ of the director from layer to layer:

$$\tilde{F}\sim b\sin^4\theta\cos^2\Delta\varphi+\tfrac{1}{4}a\sin^2(2\theta)\cos\Delta\varphi+c\sin^2\theta\sin\Delta\varphi(1+\cos\Delta\varphi), \quad (44)$$

where

$$a\equiv(3v_1+v_3)+4g_1^2+8c_f^2,$$

$$b\equiv\tfrac{3}{2}v_1-g_1^2+4c_f^2,\quad c\equiv v_5. \quad (45)$$

Most often parameters v_1 and $3v_1+v_3$ having mostly dispersion origin are negative, which promotes the formation of the synclinic phase Sm-C^* [minimum of Eq. (44) is close to $\Delta\varphi=0$ if helicity c is small]. At the same time, parameters g_1^2 and c_f^2, describing, respectively, the dipole-dipole and the dipole-quadrupole electrostatic interactions in neighboring layers, are positive, which promotes anticlinic smectic phase Sm-C_A^* [minimum of Eq. (44) is close to $\Delta\varphi=\pi$]. Thus, a competition between the dispersion and the electrostatic forces can form one of these two phases depending of the molecular structure and generate the phase transition between them with variation of temperature. It was shown in [11] that parameter $g_1^2\sim\mu^4/\cos^6\theta$, i.e., it increases with the increasing tilt angle (in other words, with the decreasing temperature). Alternatively, if the transverse molecular dipole moment μ is large or coefficient $3v_1+v_3$ is positive, then the direct transition from Sm-C_A^* to Sm-A^* can happen.

Polarization effects [the last term in Eq. (43)] promote the frustration between Sm-C_A^* and Sm-C^*, which was proposed by Isozaki *et al.* [8,9], leading to the formation of biaxial intermediate phases. Expanding all terms in free energy (43) in Taylor series with respect to small helical rotation angle of the *whole* unit cell of particular phase per smectic layer up to the square term and replacing it with $h\partial\varphi/\partial z$, one obtains Eq. (9) for the local free energy, where parameters f_0, K, q_0, λ, and ν are expressed in terms of parameters independent of the phase type and of the electric field in the following way:

$$\frac{f_0 t}{\sin^2\theta}\equiv\sum_{i=0}^{t-1}\left\{\sin^2\theta\left[b\cos^2\varphi_{i,i+1}+\frac{1}{2}c_2\sin(2\varphi_{i,i+1})\right]+\cos^2\theta[a\cos\varphi_{i,i+1}+a_1\cos\varphi_{i,i+2}+c_1\sin\varphi_{i,i+1}]\right\}-\sum_{i,j=0}^{t-1}\{[(c_p^2+2c_f^2)\omega_k^{\parallel}-c_f^2(\omega_{k-2}^{\parallel}+\omega_{k+2}^{\parallel})]\cos\varphi_{ij}-2c_fc_p(\omega_{k-1}^{\parallel}-\omega_{k+1}^{\parallel})\sin\varphi_{ij}\}+(c_p^2+2c_f^2)t-2c_f\sum_{i=0}^{t-1}(c_f\cos\varphi_{i,i+2}+2c_p\sin\varphi_{i,i+1})-\frac{1}{16}t\varepsilon^2\sum_{k=0}^{t-1}\omega_k^{\parallel},$$

$$\frac{Kt}{h^2\sin^2\theta}\equiv-\sum_{i=0}^{t-1}\{2\sin^2\theta[b\cos(2\varphi_{i,i+1})+c_2\sin(2\varphi_{i,i+1})]+\cos^2\theta[a\cos\varphi_{i,i+1}+4a_1\cos\varphi_{i,i+2}+c_1\sin\varphi_{i,i+1}]\}-2c_f\sum_{i,j=0}^{t-1}\{2c_f(\omega_{k-2}^{\parallel}+\omega_{k+2}^{\parallel})\cos\varphi_{ij}+c_p(\omega_{k-1}^{\parallel}-\omega_{k+1}^{\parallel})\sin\varphi_{ij}\}+4c_f\sum_{i=0}^{t-1}(2c_f\cos\varphi_{i,i+2}+c_p\sin\varphi_{i,i+1}),$$

$$\frac{Kq_0t}{h\sin^2\theta}\equiv-\sum_{i=0}^{t-1}\{\sin^2\theta[-b\sin(2\varphi_{i,i+1})+c_2\cos(2\varphi_{i,i+1})]+\cos^2\theta[-a\sin\varphi_{i,i+1}-2a_1\sin\varphi_{i,i+2}+c_1\cos\varphi_{i,i+1}]\}+2c_f\sum_{i,j=0}^{t-1}\{c_f(\omega_{k-2}^{\parallel}-\omega_{k+2}^{\parallel})\sin\varphi_{ij}-c_p(\omega_{k-1}^{\parallel}+\omega_{k+1}^{\parallel})\cos\varphi_{ij}\}-4c_f\sum_{i=0}^{t-1}(c_f\sin\varphi_{i,i+2}-c_p\cos\varphi_{i,i+1}),$$

$$\frac{\lambda}{\beta\mu} = \frac{1}{2t}|c_p|\sin\theta\left|1-\sum_{k=0}^{t-1}\omega_k^{\parallel}\right|\left|\sum_{i=0}^{t-1}\cos\varphi_i^0\right|,$$

$$\frac{\nu}{\beta^2\mu^2} \equiv \frac{1}{16}\sin^2\theta\left[\frac{1}{t}\sum_{i,j=0}^{t-1}\omega_k^{\perp}\cos\varphi_{ij}^0 - 2\left(1+\sum_{k=0}^{t-1}\omega_k^{\parallel}\right)\right] + \frac{1}{16}\sum_{k=0}^{t-1}\Delta\omega_k^{\parallel}, \quad (46)$$

where index $k \equiv |j-i|$; angles φ_i^0 describe the azimuthal orientation of tilts within the Ising-like prototype of the unit cell of the phase, i.e., may be equal to zero or π only; angles φ_{ij} are the azimuthal differences between the tilt directions in layers j and i including 3D distortion from Ising-like prototype, but excluding helical rotation; and angles φ_{ij}^0 are the differences between their Ising-like prototypes.

In the manner described in Sec. III one can estimate the evolution of any tilted smectic phase in the electric field. If, in addition, one compares the free energies of various phases [determined by Eq. (18) in the deformed helical phases or directly by Eq. (9) with $\partial\varphi/\partial z=0$ in the unwound phases], one can obtain the general electric field–temperature phase diagram.

Our theoretical electric field–temperature phase diagram is presented in Fig. 13(a) for some typical set of molecular parameters, for which the largest number of intermediate phases is observed [12]. Black thin lines correspond to the transition borders between phases with different q_T's. The solid red thick line detaches various helical smectic phases from unwound ones. Our investigation indicates that the helix unwinding in Sm-C_A^* and in biaxial intermediate phases appears to be the second-order phase transition (similarly to that in Sm-C^*). The dotted blue thick line detaches various monodomain phases from bidomain smectic phase. The transition from unwound Sm-C_A^* or from biaxial intermediate phases to the unwound bidomain smectic phase appears to be the first-order phase transition in the framework of our theory, while the analogous transition from monodomain Sm-C^* to bidomain smectic phase appears to be of the second order.

The experimental electric field–temperature phase diagram [76] obtained for a 4.75-μm-thick MHPBC sample with planar orientation of smectic layers is presented in Fig. 13(b). Red circles correspond to two sharp static dielectric susceptibility maximums that visualize the two thresholds in the major biaxial intermediate phases Sm-$C_A^*(q_T=1/3)$ and Sm-$C_A^*(q_T=1/2)$, while in Sm-C_A^* and in some biaxial intermediate phases, which are very close to Sm-C_A^*, only the upper threshold is visualized, because the lower one (corresponding to the unwinding process) does not change the total polarization of the sample in Sm-C_A^*. In Sm-C^*, on the contrary, only the lower threshold corresponds to sharp maximum of the dielectric susceptibility. Blue triangles in Fig. 13(b) correspond to observation of the birefringence color change from blue to green at application of the high-frequency (3 kHz) electric field with amplitude E. The stepwise birefringence color change from blue to green happens

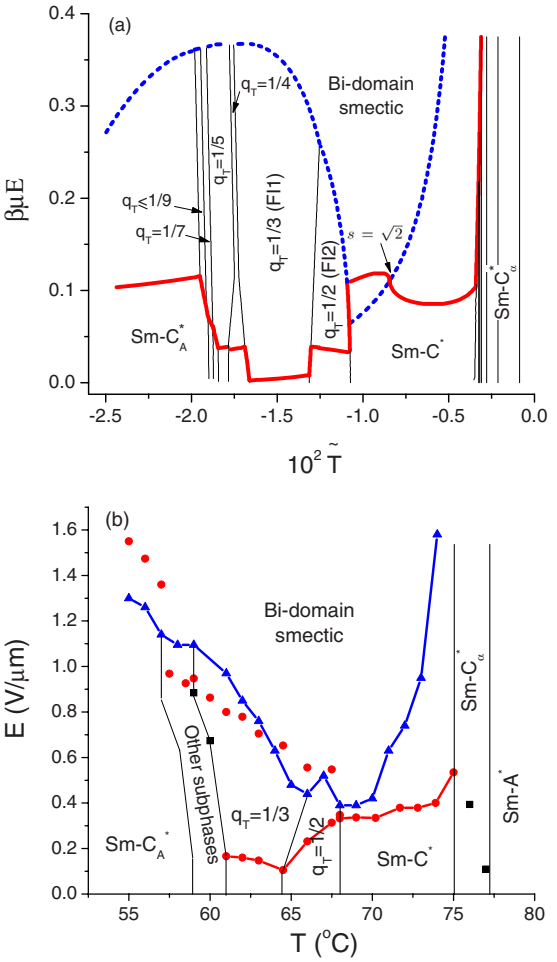

FIG. 13. (Color online) (a) Theoretical and (b) experimental phase diagrams. In (a) $\tilde{T} \equiv (T-T^*)/T^*$, T^* is the temperature of the phase transition into Sm-A^*, thin lines correspond to the transitions between phases with different q_T's, solid red thick line detaches various helical phases from unwound ones, and dotted blue thick line detaches various monodomain phases from bidomain one. In (b), obtained for 4.75-μm-thick MHPBC sample with planar orientation of smectic layers [76], red circles correspond to two static dielectric susceptibility peaks, and blue triangles correspond to observation of the dynamic (3 kHz) birefringence color change from blue to green.

in every phase in the diagram (including Sm-C^*) at the amplitudes of the electric field, which are very close to the upper static threshold. Both experimental methods reproduce the theoretical prediction with good accuracy. It is worth to mention that there are different experimental data [36,77] demonstrating even better coincidence with Fig. 13(a) than is presented in Fig. 13(b).

In Sm-C^* we have found a possibility of existence of two temperature ranges. In the higher-temperature range of Sm-C^* the order of two thresholds is the same as in Sm-C_A^* and in biaxial intermediate phases: the helical pitch diverges within the monodomain structure, and the two domains arise at some larger threshold value of the electric field. At the same time, in the lower-temperature range of Sm-C^* we found a possibility for the two thresholds to overlap: the unwinding threshold became the higher one, while the tilt

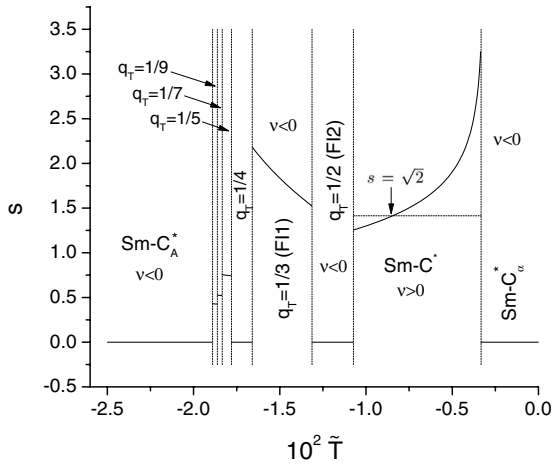

FIG. 14. Temperature dependence of parameter s, where $\tilde{T} \equiv (T-T^*)/T^*$, T^* is the temperature of the phase transition into Sm-A^*. The phase transition borders are given at $E=0$. Parameters v_1, v_3, v_5, g_1, c_p, c_f, and the components of tensors $\hat{\boldsymbol{\omega}}_k$ were calculated in the framework of molecular-statistical approach [12].

plane reorientation transformed into bidomain distortion of the helix (shown in Fig. 7) and, consequently, became the lower threshold. It was shown in Sec. III B that the point of intersection of two thresholds in the phase diagram corresponds to $s=\sqrt{2}$. Generally, the temperature dependence of parameter s in various phases is presented in Fig. 14, where the phase transition borders are given as in the corresponding diagram [Fig. 13(a)] at $E=0$. The typical values of parameter s from Fig. 14 were used in Sec. III for determination of evolution of Sm-C^*, Sm-C^*_A, and biaxial intermediate phases in the electric field.

In [35,64] it was reported about the existence of some wide-temperature ferrielectric liquid crystal (FiLC) phase in material 12OF1M7 in the temperature range between conventional intermediate phase and Sm-C^*. The authors of those publications registered the existence of two thresholds within the temperature range of the FiLC phase. However, without electric field FiLC behaved as conventional Sm-C^*, and moreover the temperature range of FiLC was too large in comparison with that of conventional ferrielectric phases. Here, we have an indication that FiLC may be the lower-temperature part of Sm-C^*, where $s<\sqrt{2}$, and where the bidomain helical structure should arise in the presence of electric field. Since in the unwound Sm-C^* polarization and birefringence continue to increase (sometimes strongly), we also have an experimental indication that two thresholds should exist in the conventional case of Sm-C^* (i.e., when $s>\sqrt{2}$) as well, but the helix unwinding (which is the lower threshold in this case) is often considered as the final step of evolution of the structure, and in many materials we have no experimental data for ferroelectric phase at larger values of the electric field, although the same publications give considerable contribution into our knowledge about antiferroelectric and intermediate phases and their behavior at high voltages.

V. CONCLUSIONS

In the present paper an evolution of ferroelectric, antiferroelectric, and ferrielectric smectic phases in the electric field is investigated. From molecular-statistical approach derived in [12] we conclude that consideration of direct influence of the electric field on the spontaneous polarization (piezoelectric effect) is not sufficient to describe this evolution, because the *magnitude* of the local polarization (per smectic layer) essentially depends on the electric field, and this dependence produces dielectriclike effect, when a contribution in the free energy proportional to the second power of the electric field arises due to anisotropy of coupling between induced polarizations in the neighboring smectic layers. This contribution, however, does not have any relation to the conventional dielectric effect, because it is not due to induction of the dipole moments, but is due to coupling of the same permanent dipole moments, which participate in spontaneous polarization in the absence of electric field. Permanent molecular transverse dipole moments exhibit essential *reorganization* in the presence of electric field, which is not normally taken into account in the phenomenological approaches.

We considered the helix distortion and unwinding in Sm-C^*, Sm-C^*_A, and biaxial intermediate phases. We obtained analytically the equations for determination of the unwinding electric field values for any of these phases taking into account both spontaneous and induced polarizations. We came to a conclusion that evolution of the helix in the electric field is described by the same analytical equations regardless of parameter q_T determining the fraction of synclinic orderings in a particular smectic phase. This evolution appeared to depend on the only quantitative parameter s [see Eq. (12)], which is a unique combination of the effective piezoelectricity of material λ, anisotropy of coupling of induced polarizations ν, elasticity constant K, and equilibrium helical wave number q_0. Parameter s effectively determines the ratio between the effect of spontaneous polarization and the effect of induced polarization at a given reduced electric field τ [see Eq. (19)]. In particular, it determines this ratio at the unwinding reduced electric field τ^*. Therefore, in addition, it effectively determines the separation between the two thresholds in the $E-T$ diagram: τ^* and τ^{**} (the latter is the critical electric field value at which the molecular tilt planes gain some contribution along or against the electric field direction due to the induced polarization effect).

The two different scenarios of the evolution of smectic structure in the electric field are possible depending on the sign of parameter ν. If parameter ν is positive (coupling of induced polarizations favors the molecular tilt planes orientation either along or against the electric field direction), the unwinding electric field is generally extended due to a competition between piezoelectric effect (which promotes perpendicular to the electric field orientation of the tilt planes) and dielectriclike effect (which promotes parallel to the electric field orientation of the tilt planes). This competition leads to a frustration between longitudinal and transverse orientations of the tilt planes in the electric field. At small values of the electric field (when the induced polarization is small) the tilt planes tend to be perpendicular to the electric field. When the electric field increases, there are two possibilities in the case $\nu>0$. If $s<\sqrt{2}$, the effect of spontaneous polarization becomes smaller than the effect of induced polarization *before* divergence of the helical pitch. In this case the bidomain helical structure with *finite* periodicity arises starting from

some critical value of electric field E^{**} (see Fig. 7), which is smaller than unwinding electric field E^{*}. If $s \geq \sqrt{2}$, the effect of spontaneous polarization becomes smaller than the effect of induced polarization only *after* divergence of the helical pitch. In this case the bidomain structure with *infinite* domain length arises starting from some critical value of electric field E^{**} (see Fig. 8), which is larger than unwinding electric field E^{*}. In particular, from Eq. (12) it follows that separation between E^{*} and E^{**} increases with the increasing equilibrium helical wave number q_0 and twist elasticity constant K. This happens because the unwinding process depends on *reduced* electric field τ, which is inversely proportional to $q_0\sqrt{K}$, while reorientation of the tilt planes depends on *real* electric field E. Here, we should note that the existence of the helical bidomain structure requires positive $E^{*}-E^{**}$, which becomes possible only at $s<\sqrt{2}$. Thus, one of the possible ways to create the wide-range helical bidomain structure in the presence of electric field is to use the short-pitch smectic material with a large elasticity constant.

If parameter ν is negative, the unwinding electric field is generally diminished, because both spontaneous and induced polarizations favor the same tendency: the molecular tilt planes prefer to be oriented perpendicular to the electric field. No bidomain structures are possible in this case.

Among various tilted smectic phases, only Sm-C^{*} demonstrates positive dielectriclike effect from induced polarizations ($\nu>0$). This effect is explained by unfavorable side-by-side ferroelectric coupling between *parallel* to the smectic layer plane projections of the induced polarizations in neighboring layers and also by favorable ferroelectric head-and-tail coupling between *normal* to the smectic layer plane projections of the same polarizations. The balance between these two couplings is shifted to the favorable one, when the tilt planes are oriented either along or against the electric field, because normal to the smectic layer projections of induced polarizations become larger in this case.

On the contrary, in Sm-C_A^{*} the normal to the smectic layer projection of induced polarization demonstrates *antiferroelectric* ordering; therefore, the tendency becomes opposite, and the dielectriclike effect from induced polarizations becomes negative ($\nu<0$). We have also shown that all the biaxial intermediate phases also demonstrate negative dielectriclike effect ($\nu<0$).

The evolution of Sm-C^{*} generally exhibits the two thresholds (both appear to be of the second-order phase transitions according to our theory). One of them (E^{*}) corresponds to the helix unwinding, when the helical pitch diverges. Another one (E^{**}) corresponds to a transition from monodomain structure to bidomain one, when the tilt planes gain some contribution either along or against the electric field. We have shown that E^{**} can indeed be smaller than E^{*} in the lower-temperature range of existence of Sm-C^{*}, while in the higher-temperature range E^{**} is typically larger than E^{*}. Coincidentally, this separation of temperature ranges corresponds to the experimental separation for "conventional" higher-temperature Sm-C^{*} phase and so-called lower-temperature FiLC phase [64]. Both "phases" demonstrate the same behavior without electric field, while in the presence of electric field the lower-temperature FiLC phase was reported to demonstrate some properties, similar to ferrielectric phases, in particular, two-threshold behavior of the helical structure. On the other hand, the temperature range of existence of FiLC was too large in comparison with typical intermediate phases, and—in addition—without electric field no phase transition between FiLC and Sm-C^{*} was observed. Here, we make a supposition that FiLC is indeed the same Sm-C^{*} where, however, the constraint $s<\sqrt{2}$ is fulfilled, so that the bidomain helical structure is supposed to arise in the electric field.

The evolution of Sm-C_A^{*} and the evolution of the intermediate biaxial phases in the electric field also exhibit the two thresholds. The helical pitch within particular phase diverges at the first (lower) threshold, which appears to be the second-order phase transition according to our theory. The second (higher) threshold appears to be the first-order phase transition from particular unwound phase into the bidomain smectic structure.

The origin of the second threshold in any tilted smectic phase is the same: positive anisotropy of coupling of induced polarizations in Sm-C^{*}. It was understood here. In particular, it was interesting to confirm experimental fact that the second threshold exists even in Sm-C^{*}, where at the first glance nothing must happen when the helix is already unwound. It was also interesting to confirm that the second threshold cuts off all the other phases (with $q_T<1$) in the diagram, so that every phase exhibits a *direct* electric-field-induced transition into the bidomain smectic phase without passing through a sequence of neighboring subphases. It was also interesting that the higher threshold is cap shaped in the lower-temperature range, so that re-entrant Sm-C^{*} may arise when the temperature decreases. This behavior does not purely correspond to our experimental diagram in Fig. 13(b). At the same time, there are different experimental data [78] reflecting this type of behavior. None of these experimental facts was explained previously.

Below, between and above the two thresholds the electric field does not change q_T (i.e., the number of synclinic and anticlinic orderings), except some peculiar points in the diagram, which are very close to the temperature phase transition borders, so that the phase transition borders are almost parallel to the "electric field" axis in the $E-T$ diagram. The birefringence measured in LC samples with planar orientation of smectic layers is almost the same between the two thresholds in every phase, which means that the structure is (almost) flat and the tilt plane is perpendicular to the electric field direction in every unwound phase. The presence of the two thresholds (demonstrating the sharpest changes in birefringence at lowest values of the electric field in the biaxial intermediate phases) outlines the importance of investigation of complex smectic phases from technological point of view. At the same time, molecular-statistical approach to the description of entire set of tilted smectic phases essentially used in the present study paves the systematic way to investigation of new perspectives in smectic materials.

ACKNOWLEDGMENTS

The author is grateful to A. Fukuda, A. V. Kaznacheev, E. P. Pozhidaev, and N. M. Shtykov for fruitful discussions and

to K. A. Pimenov for help. I gratefully acknowledge the support of Russian Federal Agency of Education (Project No. P1430), Russian Federal Agency of Science and Innovations (Project No. 02.740.11.5166), and Russian Foundation for Basic Research (Projects No. 09-03-92105, No. 10-03-13305, and No. 10-03-90016).

APPENDIX A: VARIATION OF THE FREE-ENERGY FUNCTIONAL

Let us variate the free-energy functional $\mathcal{F} \equiv \int_0^p F(\varphi, \varphi')dz$, where $\varphi = \varphi(z)$ is the azimuthal distribution of molecular tilt planes along the z axis, which is perpendicular to the smectic layer planes, and $\varphi' = \varphi'(z) = \partial\varphi/\partial z$. This variation can be written in the following form:

$$\delta\mathcal{F} = \int_0^p \left\{ \frac{\partial F}{\partial \varphi}\delta\varphi + \frac{\partial F}{\partial \varphi'}\delta\varphi' \right\} dz = 0. \tag{A1}$$

The integral over the second term in Eq. (A1) can be written as follows:

$$\int_0^p \frac{\partial F}{\partial \varphi'}\delta\varphi' dz = \frac{\partial F}{\partial \varphi'}\delta\varphi|_0^p - \int_0^p \delta\varphi \frac{d}{dz}\left(\frac{\partial F}{\partial \varphi'}\right) dz. \tag{A2}$$

Since functional F is periodical with period p, the first term in Eq. (A2) is equal to zero. Then substituting Eq. (A2) into Eq. (A1), one obtains

$$\delta\mathcal{F} = \int_0^p \left\{ \frac{\partial F}{\partial \varphi} - \frac{d}{dz}\left(\frac{\partial F}{\partial \varphi'}\right) \right\} \delta\varphi dz = 0. \tag{A3}$$

Since Eq. (A3) is valid for *any* variation $\delta\phi$, then the expressions in figure brackets in Eq. (A3) must be separately equal to zero. This yields the equation of state

$$\frac{d}{dz}\left(\frac{\partial F}{\partial \varphi'}\right) = \frac{\partial F}{\partial \varphi}. \tag{A4}$$

Now let us consider the local free energy F as a function of coordinate z. Then one obtains for the total derivative of F with respect to z

$$\frac{dF}{dz} = \frac{\partial F}{\partial \varphi}\frac{d\varphi}{dz} + \frac{\partial F}{\partial \varphi'}\frac{d\varphi'}{dz}. \tag{A5}$$

Substituting Eq. (A4) into Eq. (A5), one obtains

$$\frac{dF}{dz} = \varphi' \frac{d}{dz}\left(\frac{\partial F}{\partial \varphi'}\right) + \frac{d\varphi'}{dz}\frac{\partial F}{\partial \varphi'} = \frac{d}{dz}\left\{ \varphi' \frac{\partial F}{\partial \varphi'} \right\}, \tag{A6}$$

from where it follows that

$$\frac{d}{dz}\left\{ \varphi' \frac{\partial F}{\partial \varphi'} - F \right\} = 0, \tag{A7}$$

and, thus,

$$\varphi' \frac{\partial F}{\partial \varphi'} - F = \text{const}. \tag{A8}$$

Let us write the local free energy F in the following phenomenological form:

$$F = f_0(\varphi) + f_1(\varphi)\varphi' + f_2(\varphi)\varphi'^2, \tag{A9}$$

where $f_i(\phi)$ are some functions of azimuthal angle ϕ. Then from Eq. (A8) it follows that

$$f_2(\varphi)\varphi'^2 - f_0(\varphi) = \text{const}. \tag{A10}$$

In particular, for the free energy (9) one obtains equation of state (10) (see Sec. III A), where $1/k^2$ is some constant with respect to coordinate z, which, however may depend on the dimensionless electric field E.

APPENDIX B: INTEGRATION OF SOLUTION FOR THE LOCAL FREE ENERGY OVER A PERIOD

Substituting Eq. (10) into Eq. (9) and collecting the corresponding terms, one obtains

$$\frac{F}{\rho k_B T} \approx f_0 - Kq_0\frac{\partial\varphi}{\partial z} + |\nu|E^2\left\{ \frac{K}{|\nu|E^2}\left(\frac{\partial\varphi}{\partial z}\right)^2 - \frac{1}{k^2} \right\}. \tag{B1}$$

Integrating local free energy $F(\varphi, \partial\varphi/\partial z)$ over period p with respect to coordinate z and selecting positive variation of φ along positive direction z, one obtains

$$\frac{1}{\rho k_B T}\int_0^p F(\varphi, \partial\varphi/\partial z)dz = pf_0 - 2\pi Kq_0 + |\nu|E^2\left\{ \frac{K}{|\nu|E^2}\int_0^p \frac{\partial\varphi}{\partial z}d\varphi - \frac{1}{k^2}\int_0^p \left(\frac{\partial\varphi}{\partial z}\right)^{-1} d\varphi \right\}. \tag{B2}$$

Substituting $\partial\varphi/\partial z$ from Eq. (11) into Eq. (B2), one obtains Eq. (13).

APPENDIX C: MINIMIZATION OF REDUCED FREE ENERGY f WITH RESPECT TO PARAMETER $k(E)$

Minimization of reduced free energy (16) yields

$$\frac{1}{2\rho|\nu|E^2 k_B T}\frac{df}{dk} = \frac{1}{k^3} + \frac{1}{kG_1}\frac{d}{dk}\left(\frac{G_2}{k}\right) + \left\{ \frac{G_2}{k} - \frac{2\pi}{\tau} \right\}\frac{d}{dk}\left(\frac{1}{kG_1}\right) = 0. \tag{C1}$$

Taking into account definitions of integrals G_1 and G_2 [Eq. (14)], one obtains for derivatives in the second and third terms in Eq. (C1)

$$\frac{d}{dk}\left(\frac{G_2}{k}\right) = -\frac{G_1}{k^2}, \tag{C2}$$

$$\frac{d}{dk}\left(\frac{1}{kG_1}\right) = -\frac{1}{k^2G_1^2}\int_0^{2\pi}\frac{1}{(1-k_0^2\cos\varphi \mp k^2\sin^2\varphi)^{3/2}}d\varphi. \tag{C3}$$

Substituting Eq. (C2) into Eq. (C1) and collecting the corresponding terms, one obtains

$$\frac{1}{2\rho|\nu|E^2k_BT}\frac{df}{dk} = \left\{\frac{G_2}{k} - \frac{2\pi}{\tau}\right\}\frac{d}{dk}\left(\frac{1}{kG_1}\right) = 0. \tag{C4}$$

From Eq. (C3) it follows that the derivative in the right-hand side of Eq. (C4) is never equal to zero in the range of k, where integral G_1 is finite, and thus the expression in figure brackets in the right-hand side of Eq. (C4) should be separately equal to zero, and one obtains Eq. (17) for determination of k.

[1] A. D. L. Chandani, Y. Ouchi, H. Takezoe, A. Fukuda, K. Terashima, K. Furukawa, and A. Kishi, Jpn. J. Appl. Phys., Part 2 **28**, L1261 (1989).
[2] A. D. L. Chandani, E. Gorecka, Y. Ouchi, H. Takezoe, and A. Fukuda, Jpn. J. Appl. Phys., Part 2 **28**, L1265 (1989).
[3] E. Gorecka, A. Chandani, Y. Ouchi, H. Takezoe, and A. Fukuda, Jpn. J. Appl. Phys., Part 1 **29**, 131 (1990).
[4] J. Lee, Y. Ouchi, H. Takezoe, A. Fukuda, and J. Watanabe, J. Phys.: Condens. Matter **2**, SA271 (1990).
[5] H. Takezoe, J. Lee, Y. Ouchi, and A. Fukuda, Mol. Cryst. Liq. Cryst. **202**, 85 (1991).
[6] J. Lee, A. D. L. Chandani, K. Itoh, Y. Ouchi, H. Takezoe, and A. Fukuda, Jpn. J. Appl. Phys., Part 1 **29**, 1122 (1990).
[7] N. Okabe, Y. Suzuki, I. Kawamura, T. Isozaki, H. Takezoe, and A. Fukuda, Jpn. J. Appl. Phys., Part 2 **31**, L793 (1992).
[8] T. Isozaki, T. Fujikawa, H. Takezoe, A. Fukuda, T. Hagiwara, Y. Suzuki, and I. Kawamura, Jpn. J. Appl. Phys., Part 2 **31**, L1435 (1992).
[9] T. Isozaki, T. Fujikawa, H. Takezoe, A. Fukuda, T. Hagiwara, Y. Suzuki, and I. Kawamura, Phys. Rev. B **48**, 13439 (1993).
[10] A. V. Emelyanenko and M. A. Osipov, Phys. Rev. E **68**, 051703 (2003).
[11] A. V. Emelyanenko, A. Fukuda, and J. K. Vij, Phys. Rev. E **74**, 011705 (2006).
[12] A. V. Emelyanenko, Eur. Phys. J. E **28**, 441 (2009).
[13] V. P. Panov, N. M. Shtykov, A. Fukuda, J. K. Vij, Y. Suzuki, R. A. Lewis, M. Hird, and J. W. Goodby, Phys. Rev. E **69**, 060701(R) (2004).
[14] N. M. Shtykov, A. D. L. Chandani, A. V. Emelyanenko, A. Fukuda, and J. K. Vij, Phys. Rev. E **71**, 021711 (2005).
[15] A. D. L. Chandani, N. M. Shtykov, V. P. Panov, A. V. Emelyanenko, A. Fukuda, and J. K. Vij, Phys. Rev. E **72**, 041705 (2005).
[16] Y. Takanishi, K. Hiraoka, V. K. Agrawal, H. Takezoe, A. Fukuda, and M. Matsushita, Jpn. J. Appl. Phys., Part 1 **30**, 2023 (1991).
[17] K. Hiraoka, Y. Takanishi, K. Scarp, H. Takezoe, and A. Fukuda, Jpn. J. Appl. Phys., Part 2 **30**, L1819 (1991).
[18] K. Hiraoka, Y. Takanishi, H. Takezoe, A. Fukuda, T. Isozaki, Y. Suzuki, and I. Kawamura, Jpn. J. Appl. Phys., Part 1 **31**, 3394 (1992).
[19] T. Isozaki, K. Hiraoka, Y. Takanishi, H. Takezoe, A. Fukuda, Y. Suzuki, and I. Kawamura, Liq. Cryst. **12**, 59 (1992).
[20] M. Cepic and B. Zeks, Mol. Cryst. Liq. Cryst. **263**, 61 (1995).
[21] M. Cepic and B. Zeks, Mol. Cryst. Liq. Cryst. **301**, 221 (1997).
[22] A. Roy and N. V. Madhusudana, EPL **41**, 501 (1998).
[23] A. Roy and N. V. Madhusudana, Eur. Phys. J. E **1**, 319 (2000).
[24] V. Laux, N. Isaert, H. T. Nguyen P. Cluzeau, and C. Destrade, Ferroelectrics **179**, 25 (1996).
[25] V. Laux, N. Isaert, G. Joly, and H. T. Nguyen, Liq. Cryst. **26**, 361 (1999).
[26] V. Laux, N. Isaert, V. Faye, and H. T. Nguyen, Liq. Cryst. **27**, 81 (2000).
[27] M. Cepic and B. Zeks, Phys. Rev. Lett. **87**, 085501 (2001).
[28] M. Cepic, E. Gorecka, D. Pociecha, B. Zeks, and H. T. Nguyen, J. Chem. Phys. **117**, 1817 (2002).
[29] P. Mach, R. Pindak, A.-M. Levelut, P. Barois, H. T. Nguyen, C. C. Huang, and L. Furenlid, Phys. Rev. Lett. **81**, 1015 (1998).
[30] P. Mach, R. Pindak, A.-M. Levelut, P. Barois, H. T. Nguyen, H. Baltes, M. Hird, K. Toyne, A. Seed, J. W. Goodby, C. C. Huang, and L. Furenlid, Phys. Rev. E **60**, 6793 (1999).
[31] A.-M. Levelut and B. Pansu, Phys. Rev. E **60**, 6803 (1999).
[32] T. Akizuki, K. Miyachi, Y. Takanishi, K. Ishikawa, H. Takezoe, and A. Fukuda, Jpn. J. Appl. Phys., Part 1 **38**, 4832 (1999).
[33] P. M. Johnson, D. A. Olson, S. Pankratz, T. Nguyen, J. Goodby, M. Hird, and C. C. Huang, Phys. Rev. Lett. **84**, 4870 (2000).
[34] F. Beaubois, J. P. Marcerou, H. T. Nguyen, and J. C. Rouillon, Eur. Phys. J. E **3**, 273 (2000).
[35] N. M. Shtykov, J. K. Vij, R. A. Lewis, M. Hird, and J. W. Goodby, Phys. Rev. E **62**, 2279 (2000).
[36] N. M. Shtykov, J. K. Vij, and H. T. Nguyen, Phys. Rev. E **63**, 051708 (2001).
[37] L. S. Matkin, S. J. Watson, H. F. Gleeson, R. Pindak, J. Pitney, P. M. Johnson, C. C. Huang, P. Barois, A.-M. Levelut, G. Srajer, J. Pollmann, J. W. Goodby, and M. Hird, Phys. Rev. E **64**, 021705 (2001).
[38] A. Cady, J. A. Pitney, R. Pindak, L. S. Matkin, S. J. Watson, H. F. Gleeson, P. Cluzeau, P. Barois, A.-M. Levelut, W. Caliebe, J. W. Goodby, M. Hird, and C. C. Huang, Phys. Rev. E **64**, 050702 (2001).
[39] I. Musevic and M. Skarabot, Phys. Rev. E **64**, 051706 (2001).
[40] L. S. Hirst, S. J. Watson, H. F. Gleeson, P. Cluzeau, P. Barois, R. Pindak, J. Pitney, A. Cady, P. M. Johnson, C. C. Huang, A.-M. Levelut, G. Srajer, J. Pollmann, W. Caliebe, A. Seed, M. R. Herbert, J. W. Goodby, and M. Hird, Phys. Rev. E **65**, 041705 (2002).
[41] I. Musevic, M. Skarabot, G. Heppke, and H. T. Nguyen, Liq. Cryst. **29**, 1565 (2002).

[42] J. P. F. Lagerwall, P. Rudquist, and S. T. Lagerwall, Liq. Cryst. **30**, 399 (2003).
[43] V. P. Panov, J. K. Vij, N. M. Shtykov, S. S. Seomun, D. D. Parghi, M. Hird, and J. W. Goodby, Phys. Rev. E **68**, 021702 (2003).
[44] A. V. Emelyanenko and M. A. Osipov, Ferroelectrics **309**, 13 (2004).
[45] H. Sun, H. Orihara, and Y. Ishibashi, J. Phys. Soc. Jpn. **62**, 2706 (1993).
[46] X. Y. Wang, T. Kyu, A. M. Rudin, and P. L. Taylor, Phys. Rev. E **58**, 5919 (1998).
[47] T. Qian and P. L. Taylor, Phys. Rev. E **60**, 2978 (1999).
[48] L. A. Parry-Jones and S. J. Elston, Phys. Rev. E **63**, 050701(R) (2001).
[49] L. A. Parry-Jones and S. J. Elston, Appl. Phys. Lett. **79**, 2097 (2001).
[50] B. Rovsek, M. Cepic, and B. Zeks, Phys. Rev. E **70**, 041706 (2004).
[51] P. V. Dolganov and V. M. Zhilin, Phys. Rev. E **77**, 031703 (2008).
[52] P. G. de Gennes, Solid State Commun. **6**, 163 (1968).
[53] V. E. Dmitrienko and V. A. Belyakov, Sov. Phys. JETP **51**, 787 (1980).
[54] V. G. Chigrinov, V. A. Baikalov, E. P. Pozhidaev, L. M. Blinov, L. A. Beresnev, and A. I. Allagulov, Sov. Phys. JETP **61**, 1193 (1985).
[55] M. Glogarova, L. Lejek, J. Pavel, U. Janovec, and F. Fousek, Mol. Cryst. Liq. Cryst. **91**, 309 (1983).
[56] V. A. Belyakov and E. I. Kats, J. Exp. Theor. Phys. **93**, 380 (2001).
[57] B. Kutnjak-Urbanc and B. Zeks, Phys. Rev. E **48**, 455 (1993).
[58] B. Kutnjak-Urbanc and B. Zeks, Phys. Rev. E **52**, 3892 (1995).
[59] M. Krueger and F. Giesselmann, J. Appl. Phys. **101**, 094102 (2007).
[60] P. G. de Gennes and J. Prost, *The Physics of Liquid Crystals*, 2nd ed. (Clarendon Press, Oxford, 1993).
[61] W. Haase, D. Ganzke, and E. P. Pozhidaev, MRS Symposia Proceedings No. 599 (Materials Research Society, Pittsburg, 1999), p. 15.
[62] S. Suwa, H. Hoshi, Y. Takanishi, K. Ishikawa, H. Takezoe, and B. Zeks, Jpn. J. Appl. Phys., Part 1 **42**, 1335 (2003).
[63] S. Suwa, Y. Takanishi, H. Hoshi, K. Ishikawa, and H. Takezoe, Liq. Cryst. **30**, 499 (2003).
[64] Yu. P. Panarin, O. Kalinovskaya, J. K. Vij, and J. W. Goodby, Phys. Rev. E **55**, 4345 (1997).
[65] J. P. F. Lagerwall, Phys. Rev. E **71**, 051703 (2005).
[66] M. A. Osipov, A. Fukuda, and H. Hakoi, Proceedings of Anglo-Japanese Joint Workshop, Southampton, UK, 2000.
[67] A. Fukuda, H. Hakoi, M. Sato, and M. A. Osipov, Mol. Cryst. Liq. Cryst. **398**, 169 (2003).
[68] M. A. Osipov, A. Fukuda, and H. Hakoi, Mol. Cryst. Liq. Cryst. **402**, 9 (2003).
[69] S. A. Pikin and V. L. Indenbom, Ferroelectrics **20**, 151 (1978).
[70] S. A. Pikin and V. L. Indenbom, Usp. Fiz. Nauk **125**, 251 (1978).
[71] S. A. Pikin and V. L. Indenbom, Sov. Phys. Usp. **21**, 487 (1979).
[72] S. A. Pikin and M. A. Osipov, in *Ferroelectric Liquid Crystals*, edited by G. Goodby (Gordon and Breach, New York, 1992).
[73] R. B. Meyer, Appl. Phys. Lett. **14**, 208 (1968).
[74] W. Helfrich, Phys. Rev. Lett. **21**, 1518 (1968).
[75] F. Brochard, J. Phys. (France) **33**, 607 (1972).
[76] A. V. Emelyanenko, E. P. Pozhidaev, N. M. Shtykov, and V. E. Molkin, J. Soc. Inf. Disp. **16**, 811 (2008).
[77] A. Fukuda, Y. Takanishi, T. Isozaki, K. Ishikawa, and H. Takezoe, J. Mater. Chem. **4**, 997 (1994).
[78] Yang-Ho Na Y. Naruse, N. Fukuda, H. Orihara, A. Fajar, V. Hamplova, M. Kaspar, and M. Glogarova, Ferroelectrics **364**, 13 (2008).